Top squarks and bottom squarks in the minimal supersymmetric standard model with complex parameters

A. Bartl,[1] S. Hesselbach,[1] K. Hidaka,[2] T. Kernreiter,[1] and W. Porod[3]
[1]*Institut für Theoretische Physik, Universität Wien, A-1090 Vienna, Austria*
[2]*Department of Physics, Tokyo Gakugei University, Koganei, Tokyo 184-8501, Japan*
[3]*Institut für Theoretische Physik, Universität Zürich, CH-8057 Zürich, Switzerland*
(Received 1 December 2003; published 11 August 2004)

We present a phenomenological study of top squarks ($\tilde{t}_{1,2}$) and bottom squarks ($\tilde{b}_{1,2}$) in the minimal supersymmetric standard model (MSSM) with complex parameters A_t, A_b, μ, and M_1. In particular we focus on the *CP* phase dependence of the branching ratios of $\tilde{t}_{1,2}$ and $\tilde{b}_{1,2}$ decays. We give the formulas of the two-body decay widths and present numerical results. We find that the effect of the phases on the $\tilde{t}_{1,2}$ and $\tilde{b}_{1,2}$ decays can be quite significant in a large region of the MSSM parameter space. This could have important implications for $\tilde{t}_{1,2}$ and $\tilde{b}_{1,2}$ searches and the MSSM parameter determination in future collider experiments. We have also estimated the accuracy expected in the determination of the parameters of $\tilde{t}_i$ and $\tilde{b}_i$ by a global fit of the measured masses, decay branching ratios, and production cross sections at e^+e^- linear colliders with polarized beams. Analyzing two scenarios, we find that the fundamental parameters apart from A_t and A_b can be determined with errors of 1% to 2%, assuming an integrated luminosity of 1 ab^{-1} and a sufficiently large center of mass system (c.m.s.) energy to produce also the heavier $\tilde{t}_2$ and $\tilde{b}_2$ states. The parameter A_t can be determined with an error of 2–3%, whereas the error on A_b is likely to be of the order of 50%.

DOI: 10.1103/PhysRevD.70.035003 PACS number(s): 14.80.Ly, 12.60.Jv

I. INTRODUCTION

Supersymmetry (SUSY) is one of the most attractive and best studied extensions of the standard model (SM) [1]. With SUSY the hierarchy problem can be solved and the mass of the Higgs boson can be stabilized against radiative corrections. While this is certainly the main motivation, SUSY gives us the additional benefit of introducing potential new sources of *CP* violation [2,3]. As the tiny amount of *CP* violation in the SM is not sufficient to explain the baryon asymmetry of the Universe [4], the systematic study of all implications of the complex SUSY parameters becomes absolutely necessary.

In the present paper we study the effects of complex SUSY parameters on the phenomenology of the scalar top quark and scalar bottom quark system. Analyzing the properties of 3rd generation sfermions is particularly interesting, because of the effects of the large Yukawa couplings. Their lighter mass eigenstates may be among the light SUSY particles and they could be investigated at the Tevatron and at e^+e^- linear colliders [5–12]. At the CERN Large Hadron Collider (LHC) these states can be produced directly or in cascade decays of heavier SUSY particles [13–16]. Analyses of the decays of the 3rd generation sfermions $\tilde{t}_{1,2}$, $\tilde{b}_{1,2}$, $\tilde{\tau}_{1,2}$, and $\tilde{\nu}_\tau$ in the minimal supersymmetric standard model (MSSM) with real parameters have been performed in Refs. [17–19]. Phenomenological studies of production and decays of the 3rd generation sfermions at future e^+e^- linear colliders, again in the real MSSM, have been made in Refs. [6–9].

In the MSSM several SUSY breaking parameters and the Higgsino mass parameter μ can be complex. In a complete phenomenological analysis of production and decays of third generation sfermions one has to take into account that the SUSY parameters A_f, μ, and M_i ($i=1,2,3$) are complex in general, where A_f is the trilinear scalar coupling parameter of the sfermion $\tilde{f}_i$, and the M_1, M_2, and M_3 are the U(1), SU(2), and SU(3) gaugino mass parameters, respectively. This means that one has to study the effects of the phases of the parameters on all observables.

An unambiguous signal for the *CP* phases would be provided by a measurement of a *CP*-odd observable. For example, in the case of sfermion decays a rate asymmetry [20] and triple product correlations [21,22] have been proposed as such observables. However, since it may be difficult to measure these *CP*-odd observables of the sfermions, *CP*-even observables like decay branching ratios may also be suitable for obtaining information about the SUSY *CP* phases. For example, the decay branching ratios of the Higgs bosons depend strongly on the complex phases of the $\tilde{t}$ and $\tilde{b}$ sectors [23–25], while those of the staus $\tilde{\tau}_{1,2}$ and τ-sneutrino $\tilde{\nu}_\tau$ can be quite sensitive to the phases of the stau and gaugino-Higgsino sectors [26]. Also the Yukawa couplings of the third generation sfermions are sensitive to the SUSY phases at one-loop level [27]. Furthermore, explicit *CP* violation in the Higgs sector can be induced by $\tilde{t}$ and $\tilde{b}$ loops if the parameters A_t, A_b, and μ are complex [23,28–30]. It is found [23,25,28,31] that these *CP* phase effects could significantly influence the phenomenology of the Higgs boson sector.

The experimental upper bounds on the electric dipole moments (EDM's) of electrons, neutrons, and the ^{199}Hg and ^{205}Tl atoms may impose constraints on the size of the SUSY *CP* phases [32,33]. However, these constraints are highly model dependent. This means that the various SUSY *CP* phases need not necessarily be small. For instance, if we adopt the MSSM and assume a cancellation mechanism [34],

it turns out that the phase of μ is restricted as $|\varphi_\mu| \lesssim \pi/10$ while the phases φ_{A_f} of the A_f parameters are not constrained. On the other hand, the size of $|\varphi_\mu|$ is not constrained by the EDM's in a model where the masses of the first and second generation sfermions are large (above the TeV scale) while the masses of the third generation sfermions are small (below 1 TeV) [35]. The restrictions on φ_μ due to the electron EDM can also be circumvented if lepton flavor violating terms are present in the slepton sector [36]. Less restrictive constraints on the phases appear at the two-loop level where 3rd generation sfermion loops can contribute to the EDM's [37].

In this article we focus on the influence of the *CP* violating SUSY phases on the fermionic and bosonic two-body decay branching ratios of 3rd generation squarks $\tilde{t}_{1,2}$ and $\tilde{b}_{1,2}$. We use the MSSM as a general framework and we assume that the parameters A_t, A_b, μ, and M_1 are complex with phases φ_{A_t}, φ_{A_b}, φ_μ, and $\varphi_{\mathrm{U}(1)}$, respectively (taking $M_{2,3}$ real). We neglect flavor changing *CP* phases and assume that the squark mass matrices and trilinear scalar coupling parameters are flavor diagonal. We take into account the explicit *CP* violation in the Higgs sector. If the top squark and bottom squark decay branching ratios show an appreciable phase dependence, this would also affect the analyses of the various gluino cascade decays such as those in Ref. [15]. In Ref. [38] we have published the first results of our study. In the present paper we give the analytic expressions for the various decay widths for the complex parameters and study in detail the phase dependences of the branching ratios. We take into account the restrictions on the MSSM parameters from the experimental data on the rare decay $b \to s\gamma$ [39]. Furthermore, we give a theoretical estimate of the precision expected for the determination of the complex top squark and bottom squark parameters by measuring suitable observables including the decay branching ratios in typical future collider experiments.

In Sec. II we give the formulas necessary to calculate the $\tilde{t}_i$ and $\tilde{b}_i$ two-body decay widths in the presence of *CP* phases. In Sec. III we present our numerical results. In Sec. IV we give a theoretical estimate how precisely the complex top squark and bottom squark parameters can be determined at future collider experiments. We present our conclusions in Sec. V.

II. SQUARK MASSES, MIXING, AND DECAY WIDTHS

A. Masses and mixing in squark sector

The left-right mixing of the top squarks and bottom squarks is described by a Hermitian 2×2 mass matrix, which in the basis $(\tilde{q}_L, \tilde{q}_R)$ reads

$$\mathcal{L}_M^{\tilde{q}} = -(\tilde{q}_L^\dagger, \tilde{q}_R^\dagger) \begin{pmatrix} M^2_{\tilde{q}_{LL}} & M^2_{\tilde{q}_{LR}} \\ M^2_{\tilde{q}_{RL}} & M^2_{\tilde{q}_{RR}} \end{pmatrix} (\tilde{q}_L \tilde{q}_R), \tag{1}$$

with

$$M^2_{\tilde{q}_{LL}} = M^2_{\tilde{Q}} + (I^q_{3L} - e_q \sin^2\theta_W)\cos 2\beta m_Z^2 + m_q^2, \tag{2}$$

$$M^2_{\tilde{q}_{RR}} = M^2_{\tilde{Q}'} + e_q \sin^2\theta_W \cos 2\beta m_Z^2 + m_q^2, \tag{3}$$

$$M^2_{\tilde{q}_{RL}} = (M^2_{\tilde{q}_{LR}})^* = m_q[A_q - \mu^*(\tan\beta)^{-2I^q_{3L}}], \tag{4}$$

where m_q, e_q, and I^q_{3L} are the mass, electric charge, and weak isospin of the quark $q = b,t$. θ_W denotes the weak mixing angle, $\tan\beta = v_2/v_1$ with v_1 (v_2) being the vacuum expectation value of the Higgs field H_1^0 (H_2^0), and $M_{\tilde{Q}'} = M_{\tilde{D}}$ ($M_{\tilde{U}}$) for $q = b$ (t). $M_{\tilde{Q}}$, $M_{\tilde{D}}$, $M_{\tilde{U}}$, A_b, and A_t are the soft SUSY-breaking parameters of the top squark and bottom squark system. In the case of complex parameters μ and A_q the off-diagonal elements $M^2_{\tilde{q}_{RL}} = (M^2_{\tilde{q}_{LR}})^*$ are also complex with the phase

$$\varphi_{\tilde{q}} = \arg[M^2_{\tilde{q}_{RL}}] = \arg[A_q - \mu^*(\tan\beta)^{-2I^q_{3L}}]. \tag{5}$$

The mass eigenstates are

$$\begin{pmatrix} \tilde{q}_1 \\ \tilde{q}_2 \end{pmatrix} = \mathcal{R}^{\tilde{q}} \begin{pmatrix} \tilde{q}_L \\ \tilde{q}_R \end{pmatrix} \tag{6}$$

with the $\tilde{q}$-mixing matrix

$$\mathcal{R}^{\tilde{q}} = \begin{pmatrix} e^{i\varphi_{\tilde{q}}}\cos\theta_{\tilde{q}} & \sin\theta_{\tilde{q}} \\ -\sin\theta_{\tilde{q}} & e^{-i\varphi_{\tilde{q}}}\cos\theta_{\tilde{q}} \end{pmatrix}, \tag{7}$$

$$\cos\theta_{\tilde{q}} = \frac{-|M^2_{\tilde{q}_{LR}}|}{\sqrt{|M^2_{\tilde{q}_{LR}}|^2 + (m^2_{\tilde{q}_1} - M^2_{\tilde{q}_{LL}})^2}},$$

$$\sin\theta_{\tilde{q}} = \frac{M^2_{\tilde{q}_{LL}} - m^2_{\tilde{q}_1}}{\sqrt{|M^2_{\tilde{q}_{LR}}|^2 + (m^2_{\tilde{q}_1} - M^2_{\tilde{q}_{LL}})^2}} \tag{8}$$

and the mass eigenvalues

$$m^2_{\tilde{q}_{1,2}} = \frac{1}{2}[M^2_{\tilde{q}_{LL}} + M^2_{\tilde{q}_{RR}} \mp \sqrt{(M^2_{\tilde{q}_{LL}} - M^2_{\tilde{q}_{RR}})^2 + 4|M^2_{\tilde{q}_{LR}}|^2}],$$

$$m_{\tilde{q}_1} < m_{\tilde{q}_2}. \tag{9}$$

B. Fermionic decay widths of $\tilde{t}_i$ and $\tilde{b}_i$

In the following we give the formulas necessary to calculate the two-body decay widths of $\tilde{t}_i$ and $\tilde{b}_i$ into charginos and neutralinos in the presence of the *CP* phases. The b-$\tilde{t}_i$-$\tilde{\chi}_k^\pm$ and t-$\tilde{b}_i$-$\tilde{\chi}_k^\pm$ couplings are defined by

$$\mathcal{L}_{q\tilde{q}\tilde{\chi}^+} = g\overline{t}(\ell^{\tilde{b}}_{ij} P_R + k^{\tilde{b}}_{ij} P_L)\tilde{\chi}_j^+ \tilde{b}_i + g\overline{b}(\ell^{\tilde{t}}_{ij} P_R + k^{\tilde{t}}_{ij} P_L)\tilde{\chi}_j^{+c}\tilde{t}_i + \mathrm{H.c.}, \tag{10}$$

with

$$P_L=\frac{1}{2}(1-\gamma_5),\quad P_R=\frac{1}{2}(1+\gamma_5), \tag{11}$$

$$\ell^{\tilde{t}}_{ij}=-\mathcal{R}^{\tilde{t}*}_{i1}V_{j1}+Y_t\mathcal{R}^{\tilde{t}*}_{i2}V_{j2},\quad k^{\tilde{t}}_{ij}=\mathcal{R}^{\tilde{t}*}_{i1}Y_bU^*_{j2}, \tag{12}$$

$$\ell^{\tilde{b}}_{ij}=-\mathcal{R}^{\tilde{b}*}_{i1}U_{j1}+Y_b\mathcal{R}^{\tilde{b}*}_{i2}U_{j2},\quad k^{\tilde{b}}_{ij}=\mathcal{R}^{\tilde{b}*}_{i1}Y_tV^*_{j2}, \tag{13}$$

and

$$Y_t=\frac{m_t}{\sqrt{2}m_W\sin\beta},\quad Y_b=\frac{m_b}{\sqrt{2}m_W\cos\beta}, \tag{14}$$

where g is the $SU(2)_L$ gauge coupling and the 2×2 chargino mixing matrices U and V are defined in Eq. (A3).

The q-$\tilde{q}_i$-$\tilde{\chi}^0_k$ couplings ($q=t,b$) are defined by

$$\mathcal{L}_{q\tilde{q}\tilde{\chi}^0}=g\bar{q}(a^{\tilde{q}}_{ik}P_R+b^{\tilde{q}}_{ik}P_L)\tilde{\chi}^0_k\tilde{q}_i+\text{H.c.}, \tag{15}$$

with

$$a^{\tilde{q}}_{ik}=\sum_{n=1}^{2}(\mathcal{R}^{\tilde{q}}_{in})^*\mathcal{A}^q_{kn},\quad b^{\tilde{q}}_{ik}=\sum_{n=1}^{2}(\mathcal{R}^{\tilde{q}}_{in})^*\mathcal{B}^q_{kn}, \tag{16}$$

where

$$\mathcal{A}^q_k=\begin{pmatrix}f^q_{Lk}\\ h^q_{Rk}\end{pmatrix},\quad \mathcal{B}^q_k=\begin{pmatrix}h^q_{Lk}\\ f^q_{Rk}\end{pmatrix}, \tag{17}$$

$$f^t_{Lk}=-\frac{1}{\sqrt{2}}\left(N_{k2}+\frac{1}{3}\tan\theta_WN_{k1}\right),$$

$$f^t_{Rk}=2\sqrt{\frac{2}{3}}\tan\theta_WN^*_{k1},$$

$$h^t_{Lk}=(h^t_{Rk})^*=-Y_tN^*_{k4}, \tag{18}$$

and

$$f^b_{Lk}=\frac{1}{\sqrt{2}}\left(N_{k2}-\frac{1}{3}\tan\theta_WN_{k1}\right),$$

$$f^b_{Rk}=-\sqrt{\frac{2}{3}}\tan\theta_WN^*_{k1},$$

$$h^b_{Lk}=(h^b_{Rk})^*=-Y_bN^*_{k3}. \tag{19}$$

The 4×4 neutralino mixing matrix N is defined in Eq. (A5). The partial decay widths of $\tilde{q}_i$ ($\tilde{q}_i=\tilde{t}_i,\tilde{b}_i$) into fermionic final states then read

$$\Gamma(\tilde{q}_i\to q'+\tilde{\chi}^\pm_k)=\frac{g^2\lambda^{1/2}(m^2_{\tilde{q}_i},m^2_{q'},m^2_{\tilde{\chi}^\pm_k})}{16\pi m^3_{\tilde{q}_i}}[(|k^{\tilde{q}}_{ik}|^2+|\ell^{\tilde{q}}_{ik}|^2)\times(m^2_{\tilde{q}_i}-m^2_{q'}-m^2_{\tilde{\chi}^\pm_k})-4\,\mathrm{Re}(k^{\tilde{q}*}_{ik}\ell^{\tilde{q}}_{ik})m_{q'}m_{\tilde{\chi}^\pm_k}] \tag{20}$$

and

$$\Gamma(\tilde{q}_i\to q+\tilde{\chi}^0_k)=\frac{g^2\lambda^{1/2}(m^2_{\tilde{q}_i},m^2_q,m^2_{\tilde{\chi}^0_k})}{16\pi m^3_{\tilde{q}_i}}[(|a^{\tilde{q}}_{ik}|^2+|b^{\tilde{q}}_{ik}|^2)\times(m^2_{\tilde{q}_i}-m^2_q-m^2_{\tilde{\chi}^0_k})-4\,\mathrm{Re}(a^{\tilde{q}*}_{ik}b^{\tilde{q}}_{ik})m_qm_{\tilde{\chi}^0_k}], \tag{21}$$

with $\lambda(x,y,z)=x^2+y^2+z^2-2(xy+xz+yz)$.

C. Bosonic decay widths of $\tilde{t}_i$ and $\tilde{b}_i$

Here we show the couplings relevant for the two-body decays of $\tilde{t}_i$ and $\tilde{b}_i$ into gauge and Higgs bosons. The $\tilde{q}_i$-$\tilde{q}'_j$-$W^\pm$ couplings are defined by

$$\mathcal{L}_{\tilde{q}\tilde{q}'W}=-ig(A^W_{\tilde{b}_i\tilde{t}_j}W^+_\mu\tilde{t}^\dagger_j\overleftrightarrow{\partial^\mu}\tilde{b}_i+A^W_{\tilde{t}_i\tilde{b}_j}W^-_\mu\tilde{b}^\dagger_j\overleftrightarrow{\partial^\mu}\tilde{t}_i) \tag{22}$$

with

$$A^W_{\tilde{b}_i\tilde{t}_j}=(A^W_{\tilde{t}_j\tilde{b}_i})^*=\frac{1}{\sqrt{2}}\mathcal{R}^{\tilde{b}}_{i1}{}^*\mathcal{R}^{\tilde{t}}_{j1}. \tag{23}$$

The $\tilde{q}_i$-$\tilde{q}_j$-Z interaction Lagrangian reads

$$\mathcal{L}_{\tilde{q}\tilde{q}Z}=-igB^Z_{ij}Z_\mu\tilde{q}^\dagger_j\overleftrightarrow{\partial^\mu}\tilde{q}_i \tag{24}$$

with

$$B^Z_{ij}=\frac{1}{\cos\theta_W}\times\begin{pmatrix}I^q_{3L}\cos^2\theta_{\tilde{q}}-e_q\sin^2\theta_W & -\frac{1}{2}I^q_{3L}\sin2\theta_{\tilde{q}}e^{-i\varphi_{\tilde{q}}}\\ -\frac{1}{2}I^q_{3L}\sin2\theta_{\tilde{q}}e^{i\varphi_{\tilde{q}}} & I^q_{3L}\sin^2\theta_{\tilde{q}}-e_q\sin^2\theta_W\end{pmatrix}. \tag{25}$$

The $\tilde{q}_i$-$\tilde{q}'_j$-$H^\pm$ couplings are defined by

$$\mathcal{L}_{\tilde{q}\tilde{q}H^\pm}=g(C^H_{\tilde{t}_j\tilde{b}_i}H^+\tilde{t}^\dagger_j\tilde{b}_i+C^H_{\tilde{b}_j\tilde{t}_i}H^-\tilde{b}^\dagger_j\tilde{t}_i) \tag{26}$$

with

$$C^H_{\tilde{t}_i\tilde{b}_j}=(C^H_{\tilde{b}_j\tilde{t}_i})^*=\frac{1}{\sqrt{2}m_W}(\mathcal{R}^{\tilde{t}}G\mathcal{R}^{\tilde{b}\dagger})_{ij} \tag{27}$$

and

$$G=\begin{pmatrix} m_b^2\tan\beta+m_t^2\cot\beta-m_W^2\sin 2\beta & m_b(|A_b|e^{-i\varphi_{A_b}}\tan\beta+|\mu|e^{i\varphi_\mu}) \\ m_t(|A_t|e^{i\varphi_{A_t}}\cot\beta+|\mu|e^{-i\varphi_\mu}) & 2m_tm_b/\sin 2\beta \end{pmatrix}. \tag{28}$$

For the couplings of squarks to neutral Higgs bosons we have the Lagrangian

$$\mathcal{L}_{\tilde{q}\tilde{q}H}=-gC(\tilde{q}_k^\dagger H_i\tilde{q}_j)\tilde{q}_k^\dagger H_i\tilde{q}_j \quad (k,j=1,2) \tag{29}$$

with

$$C(\tilde{q}_k^\dagger H_i\tilde{q}_j)=\mathcal{R}^{\tilde{q}}\cdot\begin{pmatrix} C(\tilde{q}_L^\dagger H_i\tilde{q}_L) & C(\tilde{q}_L^\dagger H_i\tilde{q}_R) \\ C(\tilde{q}_R^\dagger H_i\tilde{q}_L) & C(\tilde{q}_R^\dagger H_i\tilde{q}_R) \end{pmatrix}\cdot\mathcal{R}^{\tilde{q}\dagger}, \tag{30}$$

where for $\tilde{q}=\tilde{t}$

$$C(\tilde{t}_L^\dagger H_i\tilde{t}_L)=\frac{m_t^2}{m_W\sin\beta}O_{2i}+\frac{m_Z}{\cos\theta_W}\left(\frac{1}{2}-\frac{2}{3}\sin^2\theta_W\right)\times(\cos\beta O_{1i}-\sin\beta O_{2i}), \tag{31}$$

$$C(\tilde{t}_R^\dagger H_i\tilde{t}_R)=\frac{m_t^2}{m_W\sin\beta}O_{2i}+\frac{2m_Z}{3\cos\theta_W}\sin^2\theta_W\times(\cos\beta O_{1i}-\sin\beta O_{2i}), \tag{32}$$

$$C(\tilde{t}_L^\dagger H_i\tilde{t}_R)=\frac{m_t}{2m_W\sin\beta}\{-i(\cos\beta|A_t|e^{-i\varphi_{A_t}}+\sin\beta|\mu|e^{i\varphi_\mu})O_{3i}-(|\mu|e^{i\varphi_\mu}O_{1i}-|A_t|e^{-i\varphi_{A_t}}O_{2i})\}, \tag{33}$$

$$C(\tilde{t}_R^\dagger H_i\tilde{t}_L)=[C(\tilde{t}_L^\dagger H_i\tilde{t}_R)]^*, \tag{34}$$

while for $\tilde{q}=\tilde{b}$

$$C(\tilde{b}_L^\dagger H_i\tilde{b}_L)=\frac{m_b^2}{m_W\cos\beta}O_{1i}-\frac{m_Z}{\cos\theta_W}\left(\frac{1}{2}-\frac{1}{3}\sin^2\theta_W\right)\times(\cos\beta O_{1i}-\sin\beta O_{2i}), \tag{35}$$

$$C(\tilde{b}_R^\dagger H_i\tilde{b}_R)=\frac{m_b^2}{m_W\cos\beta}O_{1i}-\frac{m_Z}{3\cos\theta_W}\sin^2\theta_W(\cos\beta O_{1i}-\sin\beta O_{2i}), \tag{36}$$

$$C(\tilde{b}_L^\dagger H_i\tilde{b}_R)=\frac{m_b}{2m_W\cos\beta}\{-i(\sin\beta|A_b|e^{-i\varphi_{A_b}}+\cos\beta|\mu|e^{i\varphi_\mu})O_{3i}-(|\mu|e^{i\varphi_\mu}O_{2i}-|A_b|e^{-i\varphi_{A_b}}O_{1i})\}, \tag{37}$$

$$C(\tilde{b}_R^\dagger H_i\tilde{b}_L)=[C(\tilde{b}_L^\dagger H_i\tilde{b}_R)]^*. \tag{38}$$

Here the 3×3 neutral Higgs mixing matrix O is defined in Eq. (A1).

The partial decay widths for $\tilde{q}_i=\tilde{t}_i,\tilde{b}_i$ into bosonic final states are then of the following forms:

$$\Gamma(\tilde{q}_i\to W^\pm+\tilde{q}_j')=\frac{g^2|A^W_{\tilde{q}_i\tilde{q}_j'}|^2\lambda^{3/2}(m^2_{\tilde{q}_i},m_W^2,m^2_{\tilde{q}_j'})}{16\pi m_W^2m^3_{\tilde{q}_i}}, \tag{39}$$

$$\Gamma(\tilde{q}_2\to Z+\tilde{q}_1)=\frac{g^2|B^Z_{21}|^2\lambda^{3/2}(m^2_{\tilde{q}_2},m_Z^2,m^2_{\tilde{q}_1})}{16\pi m_Z^2m^3_{\tilde{q}_2}}, \tag{40}$$

$$\Gamma(\tilde{q}_i\to H^\pm+\tilde{q}_j')=\frac{g^2|C^H_{\tilde{q}_j'\tilde{q}_i}|^2\lambda^{1/2}(m^2_{\tilde{q}_i},m^2_{H^\pm},m^2_{\tilde{q}_j'})}{16\pi m^3_{\tilde{q}_i}}, \tag{41}$$

$$\Gamma(\tilde{q}_2\to H_i+\tilde{q}_1)=\frac{g^2|C(\tilde{q}_1^\dagger H_i\tilde{q}_2)|^2\lambda^{1/2}(m^2_{\tilde{q}_2},m^2_{H_i},m^2_{\tilde{q}_1})}{16\pi m^3_{\tilde{q}_2}}. \tag{42}$$

III. NUMERICAL RESULTS

Before presenting numerical results, we briefly comment on the *CP* phase dependence of the $\tilde{q}_i\bar{\tilde{q}}_j$ pair production cross sections. The reaction $e^+e^-\to\tilde{q}_i\bar{\tilde{q}}_j$ $(\tilde{q}_i=\tilde{t}_i,\tilde{b}_i)$ proceeds via γ and Z exchange in the s channel. The $Z\tilde{q}_i\tilde{q}_j$ couplings are defined in Eqs. (24) and (25). The tree-level cross sections [8,9] of the reactions $e^+e^-\to\tilde{q}_i\bar{\tilde{q}}_j$ do not explicitly depend on the phases φ_μ and φ_{A_q}. In the case of the reaction $e^+e^-\to\tilde{q}_i\bar{\tilde{q}}_i$, $i=1,2$, the couplings $Z\tilde{q}_i\tilde{q}_i$ are real. In $e^+e^-\to\tilde{q}_1\bar{\tilde{q}}_2$ only the Z exchange contributes and consequently the phase $\varphi_{\tilde{q}}$ drops out in the matrix element squared. The tree-level cross sections depend only on the mass eigenvalues $m_{\tilde{q}_{1,2}}$ and on the mixing angle $\cos^2\theta_{\tilde{q}}$. Therefore, they depend only implicitly on the phases via the $\cos(\varphi_\mu+\varphi_{A_q})$ dependence of $m_{\tilde{q}_{1,2}}$ and $\theta_{\tilde{q}}$ [Eqs. (8) and (9)]. One-loop corrections to the cross sections have been calculated in Ref. [40] for real parameters. In the energy range considered here they are of the order of 10%. For complex parameters they are expected to be of the same order of magnitude. Therefore we further expect that the direct influence of the phases on the cross sections as caused by one-loop corrections would be within a few percent. These phase effects on the cross sections would be much smaller than those on the tree-level decay widths studied in this paper.

In the following we will present numerical results for the phase dependences of the $\tilde{t}_i$ and $\tilde{b}_i$ partial decay widths and

branching ratios. We calculate the partial decay widths in the Born approximation according to the expressions given in the preceding section. In some cases the one-loop SUSY QCD corrections are important. The analyses of Refs. [18,41,42] suggest that a significant part of the one-loop SUSY QCD corrections to certain partial widths of $\tilde{t}_i$ and $\tilde{b}_i$ decays (where the bottom Yukawa coupling gY_b is involved) can be incorporated by using an appropriately corrected bottom quark mass. In this spirit we calculate the tree-level widths of the $\tilde{t}_i$ and $\tilde{b}_i$ decays by using on-shell masses for the kinematic terms (such as a phase space factor) and by taking running t and b quark masses for the Yukawa couplings $gY_{t,b}$. For definiteness we take $m_t^{\rm run}(m_Z) = 150$ GeV, $m_t^{\text{on-shell}} = 175$ GeV, $m_b^{\rm run}(m_Z) = 3$ GeV, and $m_b^{\text{on-shell}} = 5$ GeV. This approach leads to an ''improved'' Born approximation which takes into account an essential part of the one-loop SUSY QCD corrections to the $\tilde{t}_i$ and $\tilde{b}_i$ partial decay widths and predicts their phase dependences more accurately than the ''naive'' tree-level calculation. The inclusion of the full one-loop corrections to the partial decay widths of $\tilde{t}_i$ and $\tilde{b}_i$ is beyond the scope of the present paper. One-loop corrections to partial decay widths of $\tilde{t}_i$ and $\tilde{b}_i$ have been given in Refs. [43,44] for real MSSM parameters and are of the order of 10%. We expect that for complex parameters they are of the same order of magnitude. In the calculation of the *CP* violating effects in the neutral Higgs sector we take the program FEYNHIGGS2.0.2 of Ref. [30], which includes the full one-loop corrections to the mass eigenvalues and mixing matrix of the neutral Higgs bosons for complex parameters. For comparison we have also used the program CPH.F of Ref. [28]. We have found agreement between the results obtained with CPH.F and the one-loop version of FEYNHIGGS2.0.2. There are small numerical differences between the results of CPH.F and the two-loop version of FEYNHIGGS2.0.2.

In the numerical analysis we impose the following conditions in order to fulfill the experimental and theoretical constraints:

(i) $m_{\tilde{\chi}_1^\pm} > 103$ GeV, $m_{\tilde{\chi}_1^0} > 50$ GeV, $m_{\tilde{t}_1,\tilde{b}_1} > 100$ GeV, $m_{\tilde{t}_1,\tilde{b}_1} > m_{\tilde{\chi}_1^0}$,

(ii) for incorporating the experimental bound on the mass of the lightest Higgs boson H_1 we use Fig. 4 of Ref. [45], replacing m_h by m_{H_1} and $\sin^2(\beta-\alpha)$ by $(O_{11}\cos\beta + O_{21}\sin\beta)^2$,[1]

(iii) $2.0\times10^{-4} < B(b\to s\gamma) < 4.5\times10^{-4}$ [39] assuming the Kobayashi-Maskawa mixing also for the squark sector,

(iv) $\Delta\rho(\tilde{t}-\tilde{b}) < 0.0012$ [46],

(v) $|A_t|^2 < 3(M_{\tilde{Q}}^2 + M_{\tilde{U}}^2 + m_2^2)$, $|A_b|^2 < 3(M_{\tilde{Q}}^2 + M_{\tilde{D}}^2 + m_1^2)$ with $m_1^2 = (m_{H^\pm}^2 + m_Z^2\sin^2\theta_W)\sin^2\beta - \frac{1}{2}m_Z^2$, $m_2^2 = (m_{H^\pm}^2 + m_Z^2\sin^2\theta_W)\cos^2\beta - \frac{1}{2}m_Z^2$.

Conditions (i) and (ii) are imposed to satisfy the experimental mass bounds from LEP [45,47,48]. Note that the *CP* violation effect reduces the $Z-Z-H_1$ coupling because H_1 can have an admixture of the *CP*-odd Higgs state a. The vertical axis of Fig. 4 of Ref. [45] describes the Z-Z-h coupling in the case of the MSSM with real parameters, which is reduced by a factor $\sin^2(\beta-\alpha)$ in comparison to the SM. The *CP* violating effects can easily be included by using $(O_{11}\cos\beta + O_{21}\sin\beta)^2$ instead of $\sin^2(\beta-\alpha)$. For the calculation of the $b\to s\gamma$ width in condition (iii) we use the formula of Ref. [49] including the $O(\alpha_s)$ corrections as given in Ref. [50]. (iv) constrains μ and $\tan\beta$ (in the squark sector). (v) is the approximate necessary condition for the tree-level vacuum stability [51].

Inspired by the gaugino mass unification we take $|M_1| = 5/3\tan^2\theta_W M_2$ and $m_{\tilde{g}} = [\alpha_s(m_{\tilde{g}})/\alpha_2]M_2$ with $m_{\tilde{g}} = M_3$. In the numerical study for $\tilde{t}_{1,2}$ decays we take $\tan\beta$, M_2, $m_{\tilde{t}_1}$, $m_{\tilde{t}_2}$, $m_{\tilde{b}_1}$, $|A_t|$, $|A_b|$, $|\mu|$, φ_{A_t}, φ_{A_b}, φ_μ, $\varphi_{\rm U(1)}$, and $m_{H^\pm}$ as input parameters, where $m_{\tilde{t}_{1,2}}$ and $m_{\tilde{b}_{1,2}}$ are the on-shell squark masses. From these input parameters we first calculate $M_{\tilde{Q}}$ and $M_{\tilde{U}}$ according to the formulas

$$M_{\tilde{Q}}^2 = \frac{1}{2}\left[m_{\tilde{t}_1}^2 + m_{\tilde{t}_2}^2 \pm \sqrt{(m_{\tilde{t}_2}^2 - m_{\tilde{t}_1}^2)^2 - 4m_t^2|A_t - \mu^*\cot\beta|^2}\right] - \left(\tfrac{1}{2} - \tfrac{2}{3}\sin^2\theta_W\right)\cos 2\beta m_Z^2 - m_t^2, \tag{43}$$

$$M_{\tilde{U}}^2 = \frac{1}{2}\left[m_{\tilde{t}_1}^2 + m_{\tilde{t}_2}^2 \mp \sqrt{(m_{\tilde{t}_2}^2 - m_{\tilde{t}_1}^2)^2 - 4m_t^2|A_t - \mu^*\cot\beta|^2}\right] - \tfrac{2}{3}\sin^2\theta_W\cos 2\beta m_Z^2 - m_t^2. \tag{44}$$

We resolve the sign ambiguity by assuming either $M_{\tilde{Q}} \geqslant M_{\tilde{U}}$ or $M_{\tilde{Q}} < M_{\tilde{U}}$: upper (lower) signs correspond to the case $M_{\tilde{Q}} \geqslant M_{\tilde{U}}$ ($M_{\tilde{Q}} < M_{\tilde{U}}$).[2] With Eq. (8) this uniquely fixes the mixing angle $\theta_{\tilde{t}}$. Next we calculate $M_{\tilde{D}}$ using $M_{\tilde{Q}}$ and $m_{\tilde{b}_1}$ and then $m_{\tilde{b}_2}$ and the mixing angle $\theta_{\tilde{b}}$ as well as the mass eigenvalues and mixing matrices of the charginos, neutralinos, and the neutral Higgs bosons. For $\tilde{b}_{1,2}$ decays we take the same input parameters with $m_{\tilde{t}_2}$ replaced by $m_{\tilde{b}_2}$ and proceed in an analogous way by interchanging $M_{\tilde{U}} \leftrightarrow M_{\tilde{D}}$.

A. Top squark decays

In this section we present numerical results for the dependence of the $\tilde{t}_1$ and $\tilde{t}_2$ partial decay widths on φ_{A_t}, φ_{A_b}, and φ_μ. In order not to vary too many parameters we fix $(m_{\tilde{t}_1}, m_{\tilde{t}_2}, m_{\tilde{b}_1}) = (350,700,170)$ GeV [(350,800,170) GeV] in the plots for the $\tilde{t}_1$ [$\tilde{t}_2$] decays. We have selected the parameters in this section such that fermionic as well as bosonic decays are allowed at the same time. In particular, the choice $m_{\tilde{b}_1} = 170$ GeV has been made to allow the decays $\tilde{t}_1 \to \tilde{b}_1 W^+$ and $\tilde{t}_1 \to \tilde{b}_1 H^+$. We consider the cases $M_{\tilde{Q}}$

[1] Note that $O_{11} \sim -\sin\alpha$, $O_{21} \sim \cos\alpha$, and $H_1 \sim h$ for $m_{H^\pm} \gg m_Z$.

[2] The hierarchy is determined by the $\tilde{t}_i$ mixing angle $\theta_{\tilde{t}}$, which can be determined by cross section measurements with polarized beams [8,9].

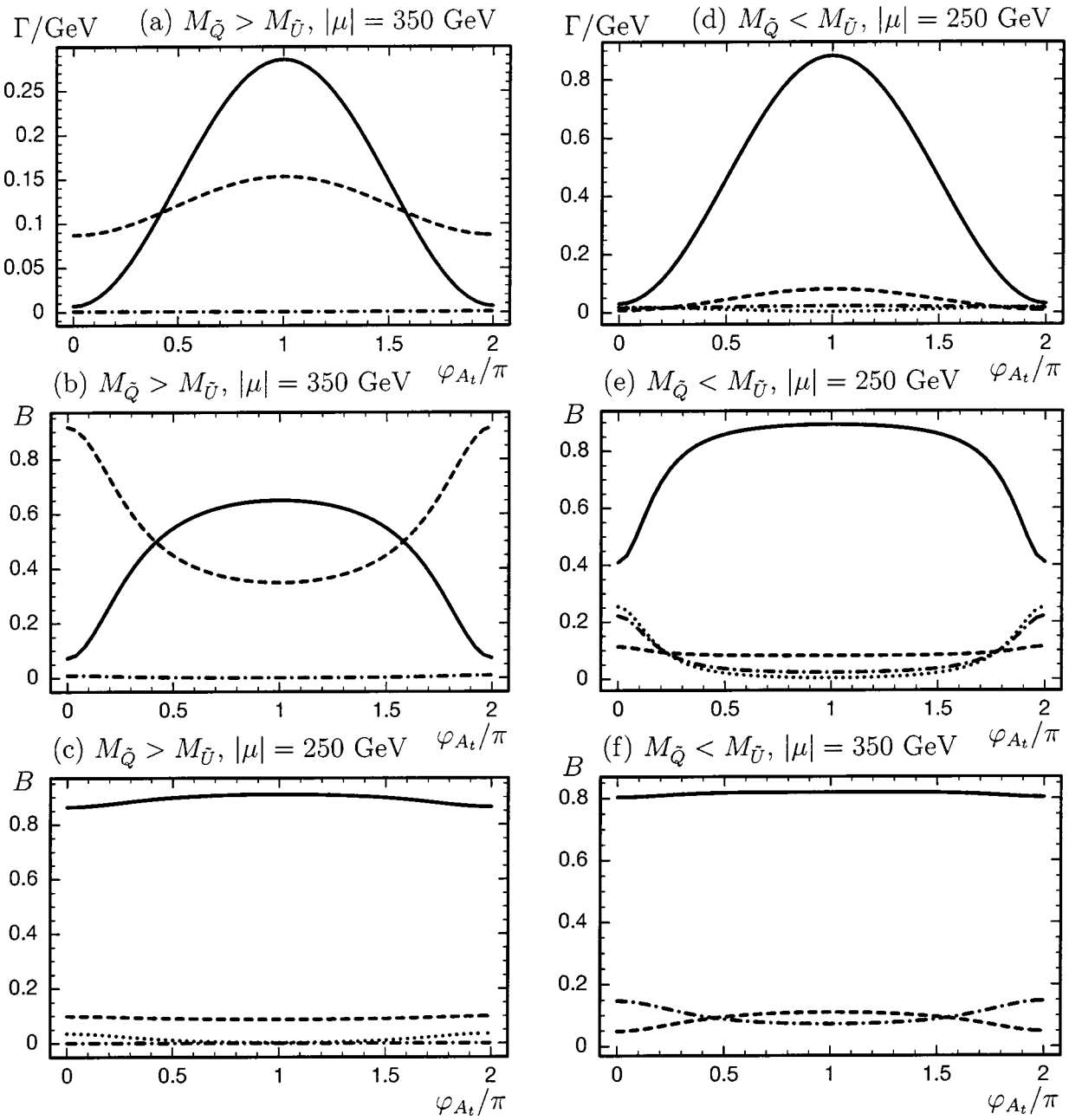

FIG. 1. (a), (d) Partial decay widths Γ and (b), (c), (e), (f) branching ratios B of the decays $\tilde{t}_1 \to \tilde{\chi}_1^+ b$ (solid), $\tilde{t}_1 \to \tilde{\chi}_2^+ b$ (dotted), $\tilde{t}_1 \to \tilde{\chi}_1^0 t$ (dashed), and $\tilde{t}_1 \to W^+ \tilde{b}_1$ (dash-dotted) for $\tan\beta = 6$, $M_2 = 300$ GeV, $|A_b| = |A_t| = 800$ GeV, $\varphi_\mu = \pi$, $\varphi_{\mathrm{U}(1)} = \varphi_{A_b} = 0$, $m_{\tilde{t}_1} = 350$ GeV, $m_{\tilde{t}_2} = 700$ GeV, $m_{\tilde{b}_1} = 170$ GeV, and $m_{H^\pm} = 900$ GeV. In (a), (b), and (f) the decay $\tilde{t}_1 \to \tilde{\chi}_2^+ b$ is kinematically forbidden.

$\geqslant M_{\tilde{U}}$ and $M_{\tilde{Q}} < M_{\tilde{U}}$, calculating the values of $M_{\tilde{Q}}$, $M_{\tilde{U}}$, and $M_{\tilde{D}}$ corresponding to $m_{\tilde{t}_1}$, $m_{\tilde{t}_2}$ and $m_{\tilde{b}_1}$ for each case, as explained above.

We show in Fig. 1 the partial decay widths and branching ratios for $\tilde{t}_1 \to \tilde{\chi}_1^+ b$, $\tilde{t}_1 \to \tilde{\chi}_2^+ b$, $\tilde{t}_1 \to \tilde{\chi}_1^0 t$, and $\tilde{t}_1 \to W^+ \tilde{b}_1$ as a function of φ_{A_t} for the parameters $\tan\beta = 6$, $M_2 = 300$ GeV, $|A_b| = |A_t| = 800$ GeV, $\varphi_\mu = \pi$, $\varphi_{\mathrm{U}(1)} = \varphi_{A_b} = 0$, $m_{H^\pm} = 900$ GeV, and two values of $|\mu| = 250$ and 350 GeV. Figures 1(a)–(c) [Figs. 1(d)–(f)] are for $M_{\tilde{Q}} > M_{\tilde{U}}$ [$M_{\tilde{Q}} < M_{\tilde{U}}$]. We first discuss Figs. 1(a) and 1(b) for the case $M_{\tilde{Q}} > M_{\tilde{U}}$ and $|\mu| = 350$ GeV. As can be seen in Fig. 1(a), $\Gamma(\tilde{t}_1 \to \tilde{\chi}_1^+ b)$, and $\Gamma(\tilde{t}_1 \to \tilde{\chi}_1^0 t)$ show quite a significant φ_{A_t} dependence. The corresponding branching ratios are shown in Fig. 1(b). For $\varphi_{A_t} \approx 0$ and 2π the decay $\tilde{t}_1 \to \tilde{\chi}_1^0 t$ dominates, whereas for $\varphi_{A_t} \approx \pi$ the decay $\tilde{t}_1 \to \tilde{\chi}_1^+ b$ has the largest branching ratio. This decay pattern can be explained in the following way: For $M_{\tilde{Q}} > M_{\tilde{U}}$ the $\tilde{t}_1$ is $\tilde{t}_R$-like. For $|\mu| > M_2$ and the parameters chosen, the chargino ($\tilde{\chi}_1^\pm$) is $\tilde{W}^\pm$-like with $m_{\tilde{\chi}_1^\pm} = 279$ GeV, so that the decay $\tilde{t}_1 \to \tilde{\chi}_1^+ b$ is suppressed by the vanishing $\tilde{t}_R$-b-$\tilde{W}^+$ coupling and by small phase space. For the parameters chosen we have $|A_t|$

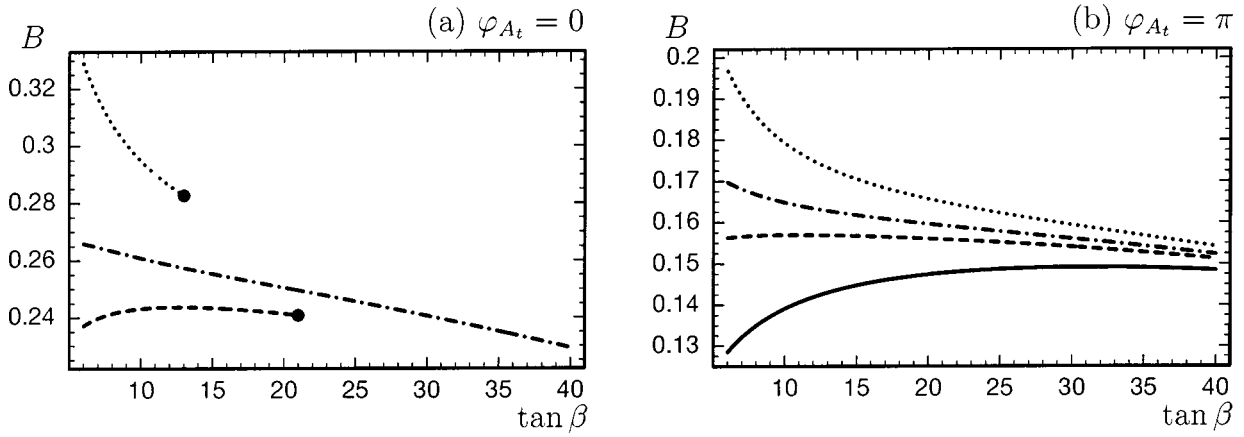

FIG. 2. Branching ratio $B(\tilde{t}_1 \to \tilde{\chi}_1^0 t)$ for $\varphi_\mu = 0$ (solid), $\pi/2$ (dashed), $5\pi/8$ (dash-dotted), and π (dotted) with $\varphi_{A_t} = 0$ (a) and π (b), $M_2 = 300$ GeV, $|\mu| = 300$ GeV, $|A_b| = |A_t| = 600$ GeV, $\varphi_{\mathrm{U}(1)} = \varphi_{A_b} = 0$, $m_{\tilde{t}_1} = 350$ GeV, $m_{\tilde{t}_2} = 700$ GeV, $m_{\tilde{b}_1} = 170$ GeV, and $m_{H^\pm} = 500$ GeV, assuming $M_{\tilde{Q}} > M_{\tilde{U}}$. In (a) the case $\varphi_\mu = 0$ is excluded by the limit $B(b \to s\gamma) < 4.5 \times 10^{-4}$, and the lines for $\varphi_\mu = \pi/2$ and $\varphi_\mu = \pi$ end in full circles beyond which $B(b \to s\gamma) > 4.5 \times 10^{-4}$ for $\tan\beta \gtrsim 21$ and $B(b \to s\gamma) < 2.0 \times 10^{-4}$ for $\tan\beta \gtrsim 13$, respectively.

$\gg |\mu|/\tan\beta$; therefore $|M^2_{\tilde{t}RL}|$ and hence $\theta_{\tilde{t}}$ depend only weakly on φ_{A_t}. However, we have $\varphi_{\tilde{t}} \approx \varphi_{A_t}$ [see Eq. (5)], therefore $\Gamma(\tilde{t}_1 \to \tilde{\chi}_1^+ b)$ behaves like $1 - \cos\varphi_{A_t}$: the leading coupling term in this decay is $\ell^{\tilde{t}}_{11} = -e^{-i\varphi_{\tilde{t}}} \cos\theta_t V_{11} + \sin\theta_t Y_t V_{12}$ [Eq. (12)], which consists of two terms of comparable size, the phase $\varphi_{\tilde{t}}$ ($\approx \varphi_{A_t}$) entering only in one of the two terms. $\Gamma(\tilde{t}_1 \to \tilde{\chi}_1^+ b)$ is very small for $\varphi_{A_t} = 0$ and 2π because the two terms nearly cancel each other. The φ_{A_t} dependence of $\Gamma(\tilde{t}_1 \to \tilde{\chi}_1^0 t)$ is less pronounced compared to $\Gamma(\tilde{t}_1 \to \tilde{\chi}_1^+ b)$ due to a more complex coupling structure [Eqs. (16) and (17)]. For this reason $B(\tilde{t}_1 \to \tilde{\chi}_1^0 t)$ dominates for $\varphi_{A_t} \lesssim 0.4\pi$ and $\varphi_{A_t} \gtrsim 1.6\pi$, whereas $B(\tilde{t}_1 \to \tilde{\chi}_1^+ b)$ is larger for $0.4\pi \lesssim \varphi_{A_t} \lesssim 1.6\pi$. The branching ratio of $\tilde{t}_1 \to W^+ \tilde{b}_1$ is strongly suppressed for this set of parameters with rather small $\tan\beta = 6$ for which $\tilde{b}_1$ is almost purely $\tilde{b}_R$-like. In Fig. 1(c) we plot the branching ratios for $|\mu| = 250$ GeV. In this case the lighter chargino has a mass $m_{\tilde{\chi}_1^\pm} = 230$ GeV and a significant Higgsino component. Hence the decay $\tilde{t}_1 \to \tilde{\chi}_1^+ b$ has a large phase space and large amplitude (due to the large top Yukawa coupling gY_t) and dominates independently of φ_{A_t}, resulting in a weak φ_{A_t} dependence of the branching ratios. For $|\mu| = 250$ GeV also the decay channel $\tilde{t}_1 \to \tilde{\chi}_2^+ b$ ($m_{\tilde{\chi}_2^\pm} = 336$ GeV) is open.

Figures 1(d) and 1(e) show the partial decay widths and branching ratios of $\tilde{t}_1 \to \tilde{\chi}_1^+ b$, $\tilde{\chi}_2^+ b$, $\tilde{\chi}_1^0 t$, and $W^+ \tilde{b}_1$ against φ_{A_t} for $M_{\tilde{Q}} < M_{\tilde{U}}$, $|\mu| = 250$ GeV, and the other parameters as above. In this case $\tilde{t}_1$ is $\tilde{t}_L$-like, therefore for $|\mu| = 250$ GeV [see Fig. 1(d)] $\Gamma(\tilde{t}_1 \to \tilde{\chi}_1^+ b)$ is about three times as large as for $M_{\tilde{Q}} > M_{\tilde{U}}$ and $|\mu| = 350$ GeV [Fig. 1(a)]. $\Gamma(\tilde{t}_1 \to \tilde{\chi}_1^+ b)$ behaves like $1 - \cos\varphi_{A_t}$, which is again caused by an interplay of the two terms in the leading coupling $\ell^{\tilde{t}}_{11}$ [Eq. (12)]. For $\varphi_{A_t} \approx 0$ the decay $\tilde{t}_1 \to \tilde{\chi}_1^+ b$ is suppressed and the branching ratios of $\tilde{t}_1 \to \tilde{\chi}_2^+ b$, $\tilde{t}_1 \to W^+ \tilde{b}_1$, and $\tilde{t}_1 \to \tilde{\chi}_1^0 t$ reach 25%, 22%, and 11%, respectively [Fig. 1(e)]. For $0.2\pi \lesssim \varphi_{A_t} \lesssim 1.8\pi$ the partial decay width and hence the branching ratio of $\tilde{t}_1 \to \tilde{\chi}_1^+ b$ is clearly largest. $B(\tilde{t}_1 \to \tilde{\chi}_1^0 t)$ has values around 10%. $B(\tilde{t}_1 \to W^+ \tilde{b}_1)$ is rather small because $\tilde{b}_1 \approx \tilde{b}_R$ in this case. $\tilde{t}_1 \to \tilde{\chi}_2^+ b$ is suppressed by a small phase space. In Fig. 1(f) we show the corresponding branching ratios for $M_{\tilde{Q}} < M_{\tilde{U}}$ and $|\mu| = 350$ GeV. In this case the mixing in the bottom squark sector increases and $B(\tilde{t}_1 \to W^+ \tilde{b}_1)$ reaches values around 10% even for $\varphi_{A_t} \approx \pi$. The decay $\tilde{t}_1 \to \tilde{\chi}_1^+ b$ has the largest branching ratio because $\tilde{t}_1$ is $\tilde{t}_L$-like and $\tilde{\chi}_1^+$ is almost $\tilde{W}^+$-like. Hence in this scenario all branching ratios show a less pronounced phase dependence. In the scenarios of Fig. 1 we have calculated also the $\varphi_{\mathrm{U}(1)}$ dependence of the partial decay widths and branching ratios. By inspecting Eqs. (16)–(18) one can see that only $\Gamma(\tilde{t}_1 \to \tilde{\chi}_1^0 t)$ could be sensitive to $\varphi_{\mathrm{U}(1)}$. However, for $\tan\beta = 6$ the $\varphi_{\mathrm{U}(1)}$ dependence is already rather small. This results in a weak $\varphi_{\mathrm{U}(1)}$ dependence of the branching ratios.

In Fig. 2 we show the $\tan\beta$ dependence of $B(\tilde{t}_1 \to \tilde{\chi}_1^0 t)$ for $M_2 = 300$ GeV, $|\mu| = 300$ GeV, $|A_b| = |A_t| = 600$ GeV, $\varphi_{\mathrm{U}(1)} = \varphi_{A_b} = 0$, $m_{H^\pm} = 500$ GeV, and $\varphi_\mu = 0, \pi/2, 5\pi/8, \pi$ with (a) $\varphi_{A_t} = 0$ and (b) $\varphi_{A_t} = \pi$, assuming $M_{\tilde{Q}} > M_{\tilde{U}}$. As can be seen this branching ratio is insensitive to φ_μ for $\tan\beta \gtrsim 15$. This is mainly due to the $\mu/\tan\beta$ dependence of the $\tilde{t}_L$-$\tilde{t}_R$ mixing term and the insensitivity of the masses and mixing of $\tilde{\chi}_i^0$ to φ_μ for large $\tan\beta$. Two curves in Fig. 2(a) end in full circles beyond which the experimental constraint from $B(b \to s\gamma)$ is violated: in the case $\varphi_\mu = \pi/2$ ($\varphi_\mu = \pi$), one has $B(b \to s\gamma) > 4.5 \times 10^{-4}$ [$B(b \to s\gamma) < 2.0 \times 10^{-4}$] for $\tan\beta \gtrsim 21$ ($\tan\beta \gtrsim 13$). The case $\varphi_\mu = 0$ is completely excluded for this set of parameters. However, for $\varphi_{A_t} = \pi$ [Fig. 2(b)] the constraints from $B(b \to s\gamma)$ are always fulfilled.

We have also calculated the $\tan\beta$ dependence of the branching ratios of the $\tilde{t}_1$ decays for $M_{\tilde{Q}} < M_{\tilde{U}}$. $B(\tilde{t}_1$

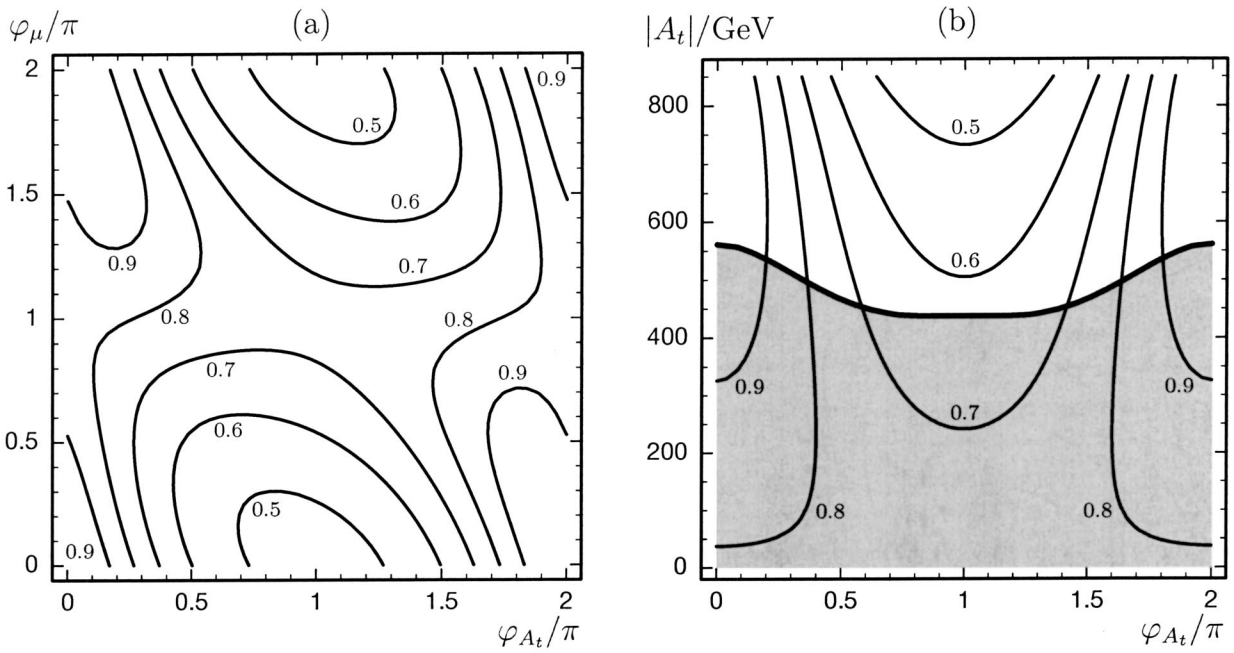

FIG. 3. Contours of $B(\tilde{t}_1 \to \tilde{\chi}_1^0 t)$ for $\tan\beta = 6$, $M_2 = 300$ GeV, $|\mu| = 500$ GeV, $\varphi_{U(1)} = \varphi_{A_b} = 0$, $m_{\tilde{t}_1} = 350$ GeV, $m_{\tilde{t}_2} = 700$ GeV, $m_{\tilde{b}_1} = 170$ GeV, $m_{H^\pm} = 600$ GeV, with (a) $|A_t| = |A_b| = 800$ GeV and (b) $\varphi_\mu = 0$, $|A_b| = |A_t|$, assuming $M_{\tilde{Q}} > M_{\tilde{U}}$. The shaded area marks the region excluded by the Higgs search at LEP [i.e., by the condition (ii)].

$\to \tilde{\chi}_1^0 t$) is smaller in this case. Therefore the effect of the phase on the $\tan\beta$ dependence is also smaller than that in Fig. 2. Moreover, for $M_{\tilde{Q}} < M_{\tilde{U}}$ the situation is different from that shown in Fig. 2, because now for $\varphi_{A_t} = 0$ the whole $\tan\beta$ range is allowed, whereas for $\varphi_{A_t} = \pi$ the constraints from $B(b \to s\gamma)$ limit the $\tan\beta$ range.

In Fig. 3(a) we show a contour plot for $B(\tilde{t}_1 \to \tilde{\chi}_1^0 t)$ as a function of φ_{A_t} and φ_μ for $\tan\beta = 6$, $M_2 = 300$ GeV, $|\mu| = 500$ GeV, $|A_t| = |A_b| = 800$ GeV, $\varphi_{U(1)} = \varphi_{A_b} = 0$, and $m_{H^\pm} = 600$ GeV, assuming $M_{\tilde{Q}} > M_{\tilde{U}}$. For the parameters chosen the φ_{A_t} dependence is stronger than the φ_μ dependence. The reason is that these phase dependences are caused mainly by the $\tilde{t}_L$-$\tilde{t}_R$ mixing term [Eq. (4)], where the φ_μ dependence is suppressed by $\cot\beta$. The φ_μ dependence is somewhat more pronounced for $\varphi_{A_t} \approx \pi$ than for $\varphi_{A_t} \approx 0, 2\pi$. In Fig. 3(b) we show the contour plot of $B(\tilde{t}_1 \to \tilde{\chi}_1^0 t)$ as a function of φ_{A_t} and $|A_t|$ for $\varphi_\mu = 0$ and $|A_t| = |A_b|$. Clearly, the φ_{A_t} dependence is stronger for larger values of $|A_t|$. For $M_{\tilde{Q}} < M_{\tilde{U}}$ we have obtained a similar behavior. Note that the phase dependences of the decay branching ratios of $\tilde{t}_1 \to \tilde{\chi}_1^+ b$, $\tilde{t}_1 \to \tilde{\chi}_2^+ b$, and $\tilde{t}_1 \to \tilde{\chi}_1^0 t$ analyzed in Figs. 1, 2, and 3 (where the decay $\tilde{t}_1 \to \tilde{b}_1 H^+$ is kinematically forbidden) would be present also for $\tilde{b}_1$ masses significantly larger than 170 GeV.

In Fig. 4 we show the contour plot for $B(\tilde{t}_1 \to \tilde{\chi}_1^+ b)$ as a function of φ_{A_t} and φ_{A_b} for $\tan\beta = 30$, $M_2 = 300$ GeV, $|\mu| = 300$ GeV, $|A_b| = |A_t| = 600$ GeV, $\varphi_\mu = \pi$, $\varphi_{U(1)} = 0$, and $m_{H^\pm} = 160$ GeV, assuming $M_{\tilde{Q}} > M_{\tilde{U}}$. As can be seen, there is a remarkable correlation between φ_{A_t} and φ_{A_b}, which turns out to be relatively independent of φ_μ. The φ_{A_t}-φ_{A_b} correlation can be explained by the behavior of the partial decay width $\Gamma(\tilde{t}_1 \to H^+ \tilde{b}_1)$, which influences all decay branching ratios. As $\tilde{b}_1 \sim \tilde{b}_R$ in this case, the relevant coupling for $\tilde{t}_1 \to H^+ \tilde{b}_1$ is $C^H_{\tilde{b}_1 \tilde{t}_1} \sim (\mathcal{R}^{\tilde{t}} G)^*_{12}$ [see Eq. (27)]. $\mathcal{R}^{\tilde{t}}$ depends on φ_{A_t} via $\tilde{t}_L$-$\tilde{t}_R$ mixing, whereas G depends on φ_{A_b} via the coupling term $m_b(A_b^* \tan\beta + \mu)$. As $\varphi_{\tilde{t}} \approx \varphi_{A_t}$ in this case, we have $(\mathcal{R}^{\tilde{t}} G)_{12} \approx e^{i(\varphi_{A_t} - \varphi_{A_b})} \cos\theta_{\tilde{t}} \cdot m_b |A_b| \tan\beta + \sin\theta_{\tilde{t}} \cdot 2 m_t m_b / \sin 2\beta$ which clearly shows the correlation between φ_{A_t} and φ_{A_b} apart from the much weaker φ_{A_t} dependence of $\theta_{\tilde{t}}$. Note that here the small value for the $\tilde{b}_1$ mass ($m_{\tilde{b}_1} = 170$ GeV) is important: for a larger $\tilde{b}_1$ mass the decay $\tilde{t}_1 \to \tilde{b}_1 H^+$ would not be allowed kinematically and hence the φ_{A_b} dependence shown in Fig. 4 would disappear.

For $M_{\tilde{Q}} < M_{\tilde{U}}$ the decay $\tilde{t}_1 \to H^+ \tilde{b}_1$ dominates for all φ_{A_t} and φ_{A_b}, resulting in a weaker phase dependence of all branching ratios. Hence also the correlation between φ_{A_t} and φ_{A_b} in $B(\tilde{t}_1 \to \tilde{\chi}_1^+ b)$ is less pronounced. However, in the scenario of Fig. 4 one has $B(b \to s\gamma) > 4.7 \times 10^{-4}$ for $M_{\tilde{Q}} < M_{\tilde{U}}$.

For the heavier top squark $\tilde{t}_2$ more decay channels are open. Besides the fermionic decay modes $\tilde{t}_2 \to \tilde{\chi}_j^+ b$, $\tilde{\chi}_i^0 t$ ($j = 1,2$; $i = 1, \ldots, 4$) there are also the bosonic decay modes $\tilde{t}_2 \to W^+ \tilde{b}_j, H^+ \tilde{b}_j, Z\tilde{t}_1, H_i \tilde{t}_1$ ($j = 1,2$; $i = 1,2,3$). In Fig. 5(a) we show the branching ratios for $\tilde{t}_2 \to \tilde{\chi}_{1,2}^+ b$ and $\tilde{t}_2 \to \tilde{\chi}_{2,3,4}^0 t$

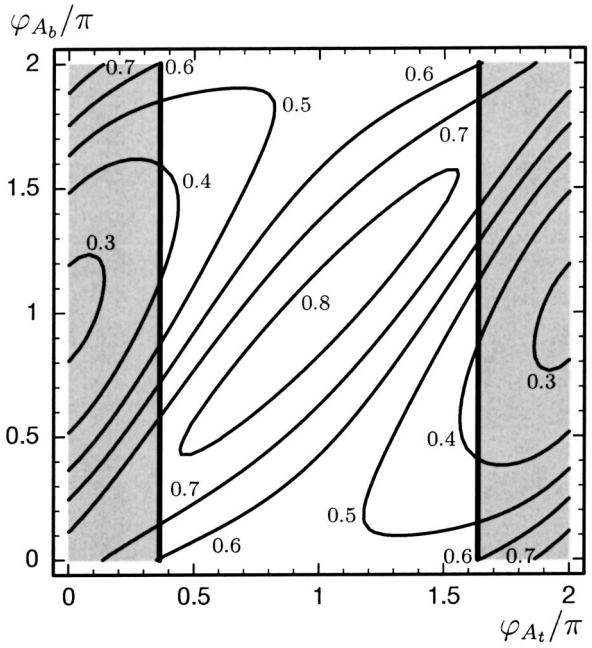

FIG. 4. Contours of $B(\tilde{t}_1 \to \tilde{\chi}_1^+ b)$ as a function of φ_{A_t} and φ_{A_b} for $\tan\beta = 30$, $M_2 = 300$ GeV, $|\mu| = 300$ GeV, $|A_b| = |A_t| = 600$ GeV, $\varphi_\mu = \pi$, $\varphi_{U(1)} = 0$, $m_{\tilde{t}_1} = 350$ GeV, $m_{\tilde{t}_2} = 700$ GeV, $m_{\tilde{b}_1} = 170$ GeV, and $m_{H^\pm} = 160$ GeV, assuming $M_{\tilde{Q}} > M_{\tilde{U}}$. The shaded areas are excluded by the experimental limit $B(b \to s\gamma) > 2.0 \times 10^{-4}$.

as a function of φ_{A_t} for $\tan\beta = 6$, $M_2 = 300$ GeV, $|\mu| = 500$ GeV, $|A_b| = |A_t| = 500$ GeV, $\varphi_\mu = \varphi_{U(1)} = \varphi_{A_b} = 0$, $m_{\tilde{t}_1} = 350$ GeV, $m_{\tilde{t}_2} = 800$ GeV, $m_{\tilde{b}_1} = 170$ GeV, and $m_{H^\pm} = 350$ GeV, assuming $M_{\tilde{Q}} > M_{\tilde{U}}$. The φ_{A_t} dependence of $B(\tilde{t}_2 \to \tilde{\chi}_{1,2}^+ b)$ is again due to a direct phase effect, because the leading coupling $\ell_{2j}^{\tilde{t}}$, $j = 1,2$ [Eq. (12)] consists of two terms, with the phase $\varphi_{\tilde{t}} (\approx \varphi_{A_t})$ entering only the factor $\mathcal{R}_{22}^{\tilde{t}}{}^*$ in the second term. Therefore, the shape of $B(\tilde{t}_2 \to \tilde{\chi}_{1,2}^+ b)$ is like $(1 \pm \cos\varphi_{A_t})$. Also the phase dependence of the branching ratios into neutralinos is mainly due to a direct phase effect. In $\Gamma(\tilde{t}_2 \to \tilde{\chi}_i^0 t)$, $i = 2,3,4$ the phase $\varphi_{\tilde{t}} (\approx \varphi_{A_t})$ enters into the second term of the couplings $a_{2i}^{\tilde{t}}$ and $b_{2i}^{\tilde{t}}$ [see Eq. (16)] via $\mathcal{R}_{22}^{\tilde{t}}{}^*$. For $\Gamma(\tilde{t}_2 \to \tilde{\chi}_2^0 t)$ the coupling $a_{22}^{\tilde{t}}$ dominates and the size of its second term is smaller than 10% of its first term. Hence the $|a_{22}^{\tilde{t}}|^2$ term in the width of Eq. (21) creates its weak phase dependence like $10 + \cos\varphi_{A_t}$. However, for $\Gamma(\tilde{t}_2 \to \tilde{\chi}_3^0 t)$ the mixing phase enters mainly into the second term of the partial width via $\mathrm{Re}(a_{23}^{\tilde{t}*} b_{23}^{\tilde{t}}) \sim \mathrm{Re}(\mathcal{R}_{22}^{\tilde{t}} \mathcal{R}_{21}^{\tilde{t}}{}^*) \sim \cos\varphi_{\tilde{t}} \sim \cos\varphi_{A_t}$, resulting in a shape like $1 + \cos\varphi_{A_t}$. For $\Gamma(\tilde{t}_2 \to \tilde{\chi}_4^0 t)$ the two terms in $a_{24}^{\tilde{t}}$ have comparable size, resulting in a strong φ_{A_t} dependence of the terms $|a_{24}^{\tilde{t}}|^2$ and $\mathrm{Re}(a_{24}^{\tilde{t}*} b_{24}^{\tilde{t}})$ in the partial width which eventually causes the branching ratio to behave like $1 - \cos\varphi_{A_t}$.

In Fig. 5(b) we show the branching ratios for the bosonic decays $\tilde{t}_2 \to Z\tilde{t}_1$ and $\tilde{t}_2 \to H_i \tilde{t}_1$ $(i = 1,2,3)$ for the same parameter values as above. The shape of $B(\tilde{t}_2 \to Z\tilde{t}_1)$ is like $1 - \cos\varphi_{A_t}$, which is solely due to the factor $|\sin 2\theta_{\tilde{t}}|^2$ [see Eq. (25)]. Quite generally, the phase dependence of $\Gamma(\tilde{t}_2 \to H_k \tilde{t}_1)$ is the result of a complicated interplay among the phase dependences of the H_k masses, the top squark mixing matrix elements $\mathcal{R}_{ij}^{\tilde{t}}$, the neutral Higgs mixing matrix elements O_{ij}, and the direct top squark–Higgs couplings of $\tilde{t}_L \tilde{t}_R \phi_{1,2}$ and $\tilde{t}_L \tilde{t}_R a$. In the present example the φ_{A_t} dependence of the partial widths $\Gamma(\tilde{t}_2 \to H_{1,2,3} \tilde{t}_1)$ is mainly due to the φ_{A_t} dependence of the factors $\mathcal{R}^{\tilde{t}}$ and $C(\tilde{t}_L^\dagger H_i \tilde{t}_R)$ in Eqs.

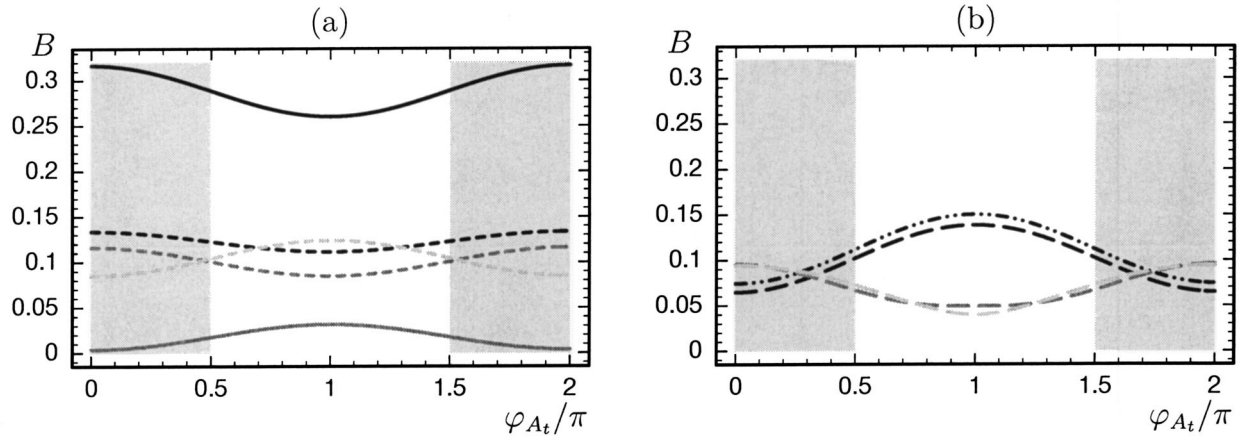

FIG. 5. φ_{A_t} dependence of branching ratios of the decays (a) $\tilde{t}_2 \to \tilde{\chi}_{1/2}^+ b$ (solid, black/gray), $\tilde{t}_2 \to \tilde{\chi}_{2/3/4}^0 t$ (dashed, black/gray/light gray) and (b) $\tilde{t}_2 \to Z\tilde{t}_1$ (dash-dot-dotted), $\tilde{t}_2 \to H_{1/2/3}\tilde{t}_1$ (long dashed, black/gray/light gray) for $\tan\beta = 6$, $M_2 = 300$ GeV, $|\mu| = 500$ GeV, $|A_b| = |A_t| = 500$ GeV, $\varphi_\mu = \varphi_{U(1)} = \varphi_{A_b} = 0$, $m_{\tilde{t}_1} = 350$ GeV, $m_{\tilde{t}_2} = 800$ GeV, $m_{\tilde{b}_1} = 170$ GeV, and $m_{H^\pm} = 350$ GeV, assuming $M_{\tilde{Q}} > M_{\tilde{U}}$. Only the decay modes with $B \gtrsim 1\%$ are shown. The shaded areas mark the region excluded by the experimental limit $B(b \to s\gamma) < 4.5 \times 10^{-4}$.

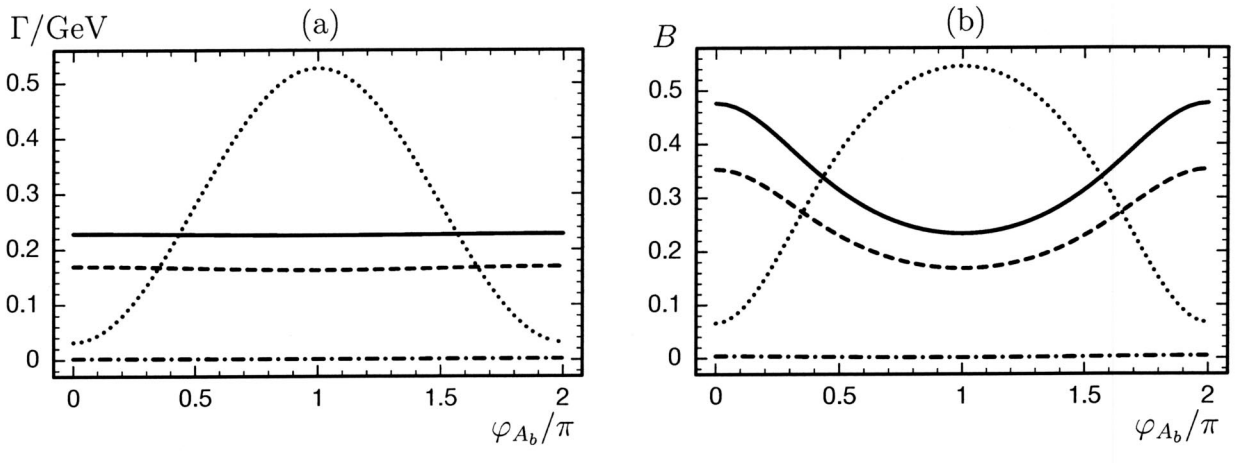

FIG. 6. φ_{A_b} dependences of (a) partial widths and (b) branching ratios of the decays $\tilde{b}_1 \to \tilde{\chi}_1^0 b$ (solid), $\tilde{b}_1 \to \tilde{\chi}_2^0 b$ (dashed), $\tilde{b}_1 \to H^- \tilde{t}_1$ (dotted), and $\tilde{b}_1 \to W^- \tilde{t}_1$ (dash-dotted) for $\tan\beta = 30$, $M_2 = 200$ GeV, $|\mu| = 300$ GeV, $|A_b| = |A_t| = 600$ GeV, $\varphi_\mu = \pi$, $\varphi_{A_t} = \varphi_{U(1)} = 0$, $m_{\tilde{b}_1} = 350$ GeV, $m_{\tilde{b}_2} = 700$ GeV, $m_{\tilde{t}_1} = 170$ GeV, and $m_{H^\pm} = 150$ GeV, assuming $M_{\tilde{Q}} > M_{\tilde{D}}$.

(30)–(34), whereas the φ_{A_t} dependence of the O_{ij} is less pronounced in this case.[3]

We have also calculated the branching ratios of the $\tilde{t}_2$ decays for $M_{\tilde{Q}} < M_{\tilde{U}}$. In this case no constraints on the φ_{A_t} range from the $B(b \to s\gamma)$ data arise in the given scenario. The φ_{A_t} dependence of $B(\tilde{t}_2 \to Z\tilde{t}_1)$ and $B(\tilde{t}_2 \to H_{1,2,3}\tilde{t}_1)$ is very similar to that shown in Fig. 5(b). The leading branching ratios are now $B(\tilde{t}_2 \to \tilde{\chi}_2^+ b)$, $B(\tilde{t}_2 \to H^+ \tilde{b}_2)$, and $B(\tilde{t}_2 \to W^+ \tilde{b}_2)$ with the values 17%, 15%, and 13% for $\varphi_{A_t} = 0, 2\pi$ and 18%, 7%, and 24% for $\varphi_{A_t} = \pi$, respectively.

Furthermore, we have calculated the $\varphi_{U(1)}$ dependence of the branching ratios of the $\tilde{t}_2$ for the scenario of Fig. 5. It turns out to be very weak because $\Gamma(\tilde{t}_2 \to \tilde{\chi}_1^0 t)$ (with $\tilde{\chi}_1^0 \sim \tilde{B}$) is suppressed in this scenario. The $\varphi_{U(1)}$ dependence stems only from that of $\Gamma(\tilde{t}_2 \to \tilde{\chi}_i^0 t)$, $i = 2,3,4$. $\tilde{\chi}_2^0$ and $\tilde{\chi}_{3,4}^0$ are W-ino- and Higgsino-dominated, respectively. Hence the masses $m_{\tilde{\chi}_{2,3,4}^0}$ and mixings N_{ij} $(i = 2,3,4)$ of $\tilde{\chi}_{2,3,4}^0$ are rather insensitive to the B-ino phase $\varphi_{U(1)}$.

B. Bottom squark decays

In the discussion of $\tilde{b}_{1,2}$ decays we fix $\tan\beta = 30$ because for small $\tan\beta$ the bottom squark mixing is too small to be phenomenologically interesting. We fix the other parameters as $m_{\tilde{b}_1} = 350$ GeV, $m_{\tilde{b}_2} = 700$ GeV, $m_{\tilde{t}_1} = 170$ GeV, $m_{H^\pm} = 150$ GeV, and $M_2 = 200$ GeV. We have chosen a relatively small value for the $\tilde{t}_1$ mass to allow for the decay $\tilde{b}_1 \to H^- \tilde{t}_1$, which has a rather strong dependence on φ_{A_b}.

In Fig. 6 we show the partial decay widths and the branching ratios of $\tilde{b}_1 \to \tilde{\chi}_{1,2}^0 b$, $H^- \tilde{t}_1$, $W^- \tilde{t}_1$ as a function of φ_{A_b} for $|\mu| = 300$ GeV, $|A_b| = |A_t| = 600$ GeV, $\varphi_\mu = \pi$, and $\varphi_{A_t} = \varphi_{U(1)} = 0$, assuming $M_{\tilde{Q}} > M_{\tilde{D}}$. In the region $0.5\pi < \varphi_{A_b} < 1.5\pi$ the decay $\tilde{b}_1 \to H^- \tilde{t}_1$ dominates. The φ_{A_b} dependence of $\Gamma(\tilde{b}_1 \to H^- \tilde{t}_1)$ is due to the term $m_b |A_b| e^{-i\varphi_{A_b}} \tan\beta$ in Eq. (28). The partial decay widths $\Gamma(\tilde{b}_1 \to \tilde{\chi}_{1,2}^0 b)$ are almost φ_{A_b} independent because the φ_{A_b} dependence of the $\tilde{b}$-mixing matrix $\mathcal{R}^{\tilde{b}}$ nearly vanishes for $\tan\beta = 30$. Hence the φ_{A_b} dependence of the branching ratios $B(\tilde{b}_1 \to \tilde{\chi}_{1,2}^0 b)$ is caused by that of the total decay width. $\Gamma(\tilde{b}_1 \to W^- \tilde{t}_1)$ is suppressed because $\tilde{b}_1 \sim \tilde{b}_R$ and $\tilde{t}_1 \sim \tilde{t}_R$ in this scenario (since also $M_{\tilde{Q}} > M_{\tilde{U}}$). For the scenario of Fig. 6 the case $M_{\tilde{Q}} < M_{\tilde{D}}$ is excluded by the experimental lower limit $B(b \to s\gamma) > 2.0 \times 10^{-4}$.

The $\varphi_{U(1)}$ dependence of the partial decay widths and branching ratios is very weak in the scenario of Fig. 6. $\varphi_{U(1)}$ enters only into $\Gamma(\tilde{b}_1 \to \tilde{\chi}_k^0 b)(k = 1,2)$, which are nearly independent of $\varphi_{U(1)}$ because $\tilde{b}_1 \sim \tilde{b}_R$ and hence mainly h_{Rk}^b in $a_{1k}^{\tilde{b}}$ and f_{Rk}^b in $b_{1k}^{\tilde{b}}$ contribute [see Eqs. (16)–(19)]. Then the phase of N_{k1}, which strongly depends on $\varphi_{U(1)}$, almost drops out in Eq. (21). Furthermore, the masses $m_{\tilde{\chi}_i^0}$ and mixing matrix elements N_{ij} of the $\tilde{\chi}_i^0$ sector are insensitive to $\varphi_{U(1)}$ for large $\tan\beta$.

For large $\tan\beta$ one expects also a significant $|A_b|$ dependence of $\Gamma(\tilde{b}_1 \to H^- \tilde{t}_1)$ [see Eq. (28)]. This can be seen in Fig. 7(a) where we show the contour plot of $B(\tilde{b}_1 \to H^- \tilde{t}_1)$ as a function of $|A_b|$ and φ_{A_b} for $|\mu| = 300$ GeV, $\varphi_\mu = \pi$, $\varphi_{A_t} = \varphi_{U(1)} = 0$, and $|A_t| = |A_b|$, assuming $M_{\tilde{Q}} > M_{\tilde{D}}$. The φ_{A_b} dependence is stronger for larger values of $|A_b|$. Although Fig. 7(a) is similar to Fig. 3(b), the $|A_b|$ and φ_{A_b} dependence in Fig. 7(a) is now caused by the coupling $m_b(A_b^* \tan\beta + \mu)$ in Eq. (28).

[3]For completeness we remark that the effect of the phase dependence of $\tilde{t}_i$-$\tilde{t}_j$-H_k couplings also shows up in processes like $e^+e^- \to \tilde{t}_1 \bar{\tilde{t}}_1 H_1$ [52].

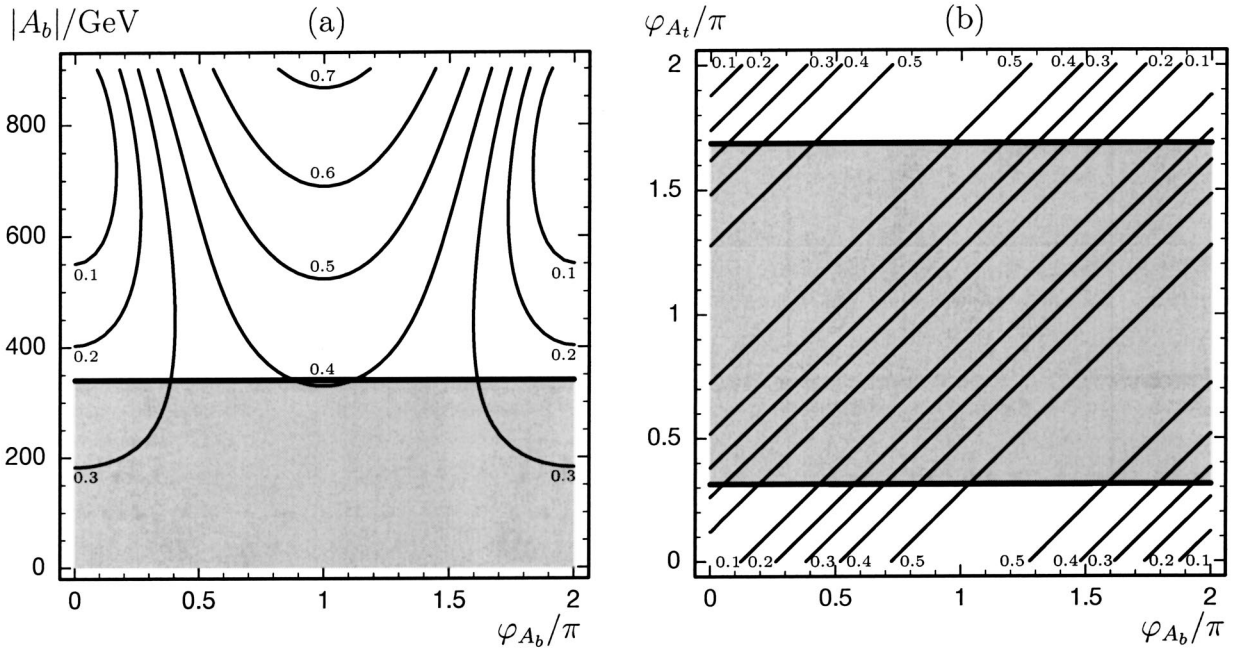

FIG. 7. Contours of $B(\tilde{b}_1 \to H^- \tilde{t}_1)$ for $\tan\beta = 30$, $M_2 = 200$ GeV, $|\mu| = 300$ GeV, $\varphi_\mu = \pi$, $\varphi_{U(1)} = 0$, $m_{\tilde{b}_1} = 350$ GeV, $m_{\tilde{b}_2} = 700$ GeV, $m_{\tilde{t}_1} = 170$ GeV, $m_{H^\pm} = 150$ GeV, and (a) $|A_b| = |A_t|$, $\varphi_{A_t} = 0$ and (b) $|A_b| = |A_t| = 600$ GeV, assuming $M_{\tilde{Q}} > M_{\tilde{D}}$. The shaded areas in (a) and (b) mark the regions excluded by the Higgs search at LEP [i.e., by the condition (ii)] and by the experimental limit $B(b \to s\gamma) > 2.0 \times 10^{-4}$, respectively.

In the case $M_{\tilde{Q}} < M_{\tilde{D}}$, we have $(\tilde{b}_1, \tilde{t}_1) \sim (\tilde{b}_L, \tilde{t}_R)$ (since also $M_{\tilde{Q}} > M_{\tilde{U}}$) and hence $C^H_{\tilde{t}_1 \tilde{b}_1} \sim m_t(A_t \cot\beta + \mu^*)$ [see Eq. (27)]. Therefore $B(\tilde{b}_1 \to H^- \tilde{t}_1)$ is nearly independent of φ_{A_b}, which leads to contour lines approximately parallel to the φ_{A_b} axis. In this case, however, nearly the whole parameter space (i.e., the region with $|A_b| \lesssim 800$ GeV) shown in Fig. 7(a) is excluded by the limit $B(b \to s\gamma) > 2.0 \times 10^{-4}$.

In Fig. 7(b) we show the contours of $B(\tilde{b}_1 \to H^- \tilde{t}_1)$ as a function of φ_{A_b} and φ_{A_t} for $|A_t| = |A_b| = 600$ GeV and the other parameters (except φ_{A_t}) as in Fig. 7(a). As can be seen, the φ_{A_b}-φ_{A_t} correlation is even stronger than that in Fig. 4 although it has the same origin as that of $B(\tilde{t}_1 \to \tilde{\chi}_1^+ b)$. Note that in the given scenario with $m_{H^\pm} = 150$ GeV the constraint on $B(b \to s\gamma)$ is only fulfilled for a limited range of φ_{A_t}. The case $M_{\tilde{Q}} < M_{\tilde{D}}$ is excluded because $B(b \to s\gamma)$ is smaller than 2.0×10^{-4} for this case. Moreover, we want to remark that even for small $\tan\beta$ the $\tilde{b}_{1,2}$ decay branching ratios can be somewhat sensitive to $\varphi_{A_{t,b}}$ and φ_μ [38].

In case of the $\tilde{b}_2$ decays more decay channels are open. In Fig. 8 we show the branching ratios for the bosonic decays $\tilde{b}_2 \to W^- \tilde{t}_{1,2}, Z\tilde{b}_1, H^- \tilde{t}_{1,2}$, and $H_{1,2,3}\tilde{b}_1$ as a function of φ_{A_b} for $|\mu| = 350$ GeV, $|A_b| = |A_t| = 600$ GeV, $\varphi_\mu = \varphi_{A_t} = \pi$, and $\varphi_{U(1)} = 0$, assuming $M_{\tilde{Q}} < M_{\tilde{D}}$. The branching ratios of the fermionic decays are nearly independent of φ_{A_b} in this scenario. The phase dependence of $\Gamma(\tilde{b}_2 \to W^- \tilde{t}_{1,2})$ and $\Gamma(\tilde{b}_2 \to Z\tilde{b}_1)$ is caused solely by the phase dependence of the squark mixing angles $\theta_{\tilde{b}}$ and $\theta_{\tilde{t}}$, which is very weak in this scenario. The strong φ_{A_b} dependence of $\Gamma(\tilde{b}_2 \to H^- \tilde{t}_{1,2})$ is caused by the term $m_b(A_b^* \tan\beta + \mu)$ in the coupling $C^H_{\tilde{t}\tilde{b}}$ [Eqs. (27) and (28)]. As $\tilde{b}_2 \sim \tilde{b}_R$ and $\varphi_{\tilde{t}} \simeq \varphi_{A_t} = \pi$ in this case, the dominating term in the coupling $C^H_{\tilde{t}\tilde{b}}$ is $(\mathcal{R}^{\tilde{t}} G)_{12} \simeq -e^{-i\varphi_{A_b}} \cos\theta_{\tilde{t}} m_b |A_b| \tan\beta + 2 \sin\theta_{\tilde{t}} m_t m_b / \sin 2\beta$ for $\tilde{b}_2 \to H^- \tilde{t}_1$ and $(\mathcal{R}^{\tilde{t}} G)_{22} \simeq -e^{-i\varphi_{A_b}} \sin\theta_{\tilde{t}} m_b |A_b| \tan\beta - 2 \cos\theta_{\tilde{t}} m_t m_b / \sin 2\beta$ for $\tilde{b}_2 \to H^- \tilde{t}_2$. Therefore, $B(\tilde{b}_2 \to H^- \tilde{t}_1)$ and $B(\tilde{b}_2 \to H^- \tilde{t}_2)$ behave like $1 + \cos\varphi_{A_b}$ and $1 - \cos\varphi_{A_b}$, respectively. As in the example for the $\tilde{t}_2$ decays (Fig. 5) the φ_{A_b} dependence of $B(\tilde{b}_2 \to H_i \tilde{b}_1)(i = 1,2,3)$ is mainly due to the phase factors explicitly appearing in Eq. (37) whereas the φ_{A_b} dependence of the O_{ij} is less pronounced. Furthermore, there is only a small mixing in the bottom squark sector with $\tilde{b}_2 \approx \tilde{b}_R$ and $\tilde{b}_1 \approx \tilde{b}_L$ in this scenario. Hence the phase dependence of $B(\tilde{b}_2 \to H_i \tilde{b}_1)$ can be explained by the phase dependence of $C(\tilde{b}_L^\dagger H_i \tilde{b}_R)$ [Eq. (37)]. It turns out that H_1 and H_3 are nearly *CP*-even Higgs bosons ($\phi_{1,2}$) with $O_{3i} \approx 0$ and $|\mu| O_{2i} \approx |A_b| O_{1i}$ $(i = 1,3)$, which results in the pronounced φ_{A_b} dependence of $B(\tilde{b}_2 \to H_{1,3} \tilde{b}_1)$. H_2 is mainly a *CP*-odd Higgs boson (a) with $O_{12} \approx O_{22} \approx 0$ and $\sin\beta |A_b| \gg \cos\beta |\mu|$, resulting in the weak φ_{A_b} dependence of $B(\tilde{b}_2 \to H_2 \tilde{b}_1)$.

We have analyzed the $\tilde{b}_2$ decay branching ratios also for $M_{\tilde{Q}} > M_{\tilde{D}}$. The φ_{A_b} dependence of $B(\tilde{b}_2 \to Z\tilde{b}_1)$ and $B(\tilde{b}_2$

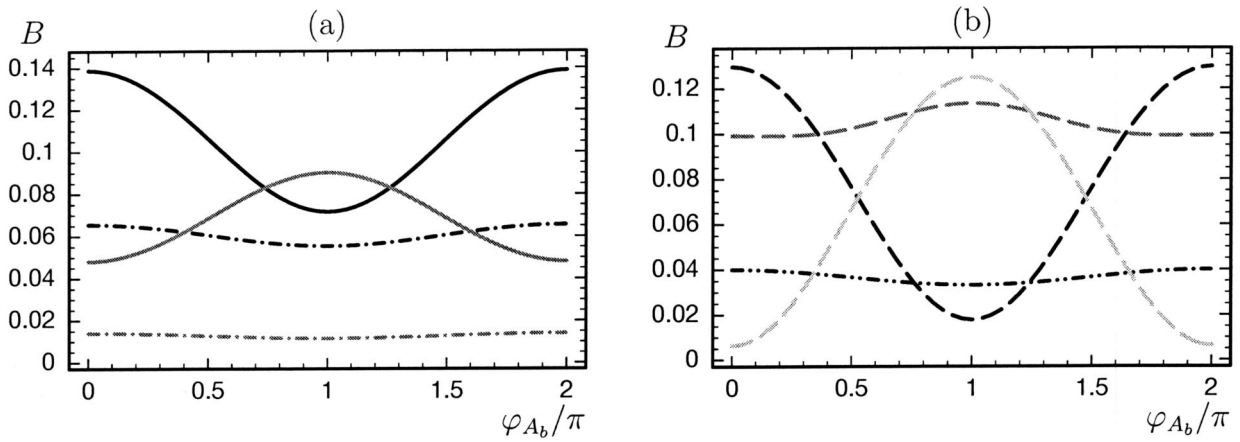

FIG. 8. φ_{A_b} dependences of the branching ratios of the bosonic decays (a) $\tilde{b}_2 \to W^- \tilde{t}_{1/2}$ (dash-dotted, black/gray), $\tilde{b}_2 \to H^- \tilde{t}_{1/2}$ (solid, black/gray), and (b) $\tilde{b}_2 \to Z\tilde{b}_1$ (dash-dot-dotted), $\tilde{b}_2 \to H_{1/2/3}\tilde{b}_1$ (long dashed, black/gray/light gray) for $\tan\beta = 30$, $M_2 = 200$ GeV, $|\mu| = 350$ GeV, $|A_b| = |A_t| = 600$ GeV, $\varphi_\mu = \varphi_{A_t} = \pi$, $\varphi_{\mathrm{U}(1)} = 0$, $m_{\tilde{b}_1} = 350$ GeV, $m_{\tilde{b}_2} = 700$ GeV, $m_{\tilde{t}_1} = 170$ GeV, and $m_{H^\pm} = 150$ GeV, assuming $M_{\tilde{Q}} < M_{\tilde{D}}$.

$\to H_{1,2,3}\tilde{b}_1$) are similar to those in Fig. 8(b), but they are smaller by a factor of ~ 3. The other branching ratios are nearly independent of φ_{A_b}. However, for the scenario of Fig. 8 the case of $M_{\tilde{Q}} > M_{\tilde{D}}$ is excluded because $B(b \to s\gamma)$ is smaller than 2.0×10^{-4} for this case.

The $\varphi_{\mathrm{U}(1)}$ dependence of the partial decay widths and branching ratios in the scenario of Fig. 8 with $M_{\tilde{Q}} < M_{\tilde{D}}$ is very weak for the same reason as in the scenario of Fig. 6 with $M_{\tilde{Q}} > M_{\tilde{D}}$ for the decays of the $\tilde{b}_1$.

IV. PARAMETER DETERMINATION

We now study to what extent one can extract the underlying parameters from measured masses, branching ratios, and cross sections. Having in mind that the squark masses are relatively large in the scenarios considered, we assume the following situations: (i) A high luminosity linear collider like TESLA can measure the masses of charginos, neutralinos, and the lightest neutral Higgs boson with high accuracy [54,55]. In the case that the squarks and the heavier Higgs bosons have masses below 500 GeV, their masses can be measured with an error of 1% and 1.5 GeV, respectively. (ii) For SUSY particles with masses larger than 500 GeV their masses can be measured at a 2 TeV e^+e^- collider, such as CLIC. The masses of heavy Higgs bosons and squarks can be measured with an error of 1% and 3%, respectively [53,57]. For the production we can get an e^- beam polarization of $P_- = 0.8$ and an e^+ beam polarization of $P_+ = 0.4$. (iii) The gluino mass can be measured at the LHC with an error of 3% [53]. (iv) m_t can be measured with an error of 0.1 GeV. In this case this error can be neglected in the fitting procedure [56]. We assume that the error on m_b can also be neglected. (v) The branching ratio of $b \to s\gamma$ can be measured within an error of 0.4×10^{-4}.

We do not take into account additional information from the LHC about the $\tilde{t}_i$ and $\tilde{b}_i$ systems, because the amount of information available strongly depends on the scenario realized in nature [58]. For example in the SPS1a scenario the decay channel $\tilde{t}_i \to b + \tilde{\chi}_1^+$ cannot be identified experimentally, because the chargino decays into a scalar tau to practically 100%. $\tilde{t}_i$ and $\tilde{b}_i$ production at the LHC will probably not give enough information about the stop and sbottom mixing angles. Moreover, the formulas for the production cross sections at the LHC, which exist in the literature, are for the real case only and do not include complex phases, which might be important for the one-loop corrections. This is the main reason why we did not consider LHC data for the stop and sbottom systems, but data from CLIC. To clarify the situation at the LHC concerning the scenarios we considered would require additional theoretical work including complex phases and further Monte Carlo studies, which are beyond the scope of this paper.

Our strategy for the parameter determination is as follows:

(i) Take a specific set of values of the underlying MSSM parameters.
(ii) Calculate the masses of $\tilde{t}_i$, $\tilde{b}_i$, $\tilde{\chi}_j^0$, $\tilde{\chi}_k^\pm$, H_ℓ, the production cross sections for $e^+e^- \to \tilde{t}_i\bar{\tilde{t}}_j$, and $e^+e^- \to \tilde{b}_i\bar{\tilde{b}}_j$, and the branching ratios of the $\tilde{t}_i$ and $\tilde{b}_i$ decays.
(iii) Regard these calculated values as real experimental data with definite errors.
(iv) Determine the underlying MSSM parameters and their errors from the ''experimental data'' by a fit using the program MINUIT [59].

We consider two scenarios in the following, one with small $\tan\beta$ and one with large $\tan\beta$. The small $\tan\beta$ scenario is characterized by $M_{\tilde{D}} = 169.6$ GeV, $M_{\tilde{U}} = 408.8$ GeV, $M_{\tilde{Q}} = 623.0$ GeV, $|A_t| = |A_b| = 800$ GeV, $\varphi_{A_t} = \varphi_{A_b} = \pi/4$, $\varphi_{U(1)} = 0$, $M_2 = 300$ GeV, $\mu = -350$ GeV, $\tan\beta = 6$, $m_{\tilde{g}} = 1000$ GeV, and $m_{H^\pm} = 900$ GeV. (Here we do not assume the unification relation between $m_{\tilde{g}}$ and M_2.) The resulting masses and their assumed experimental errors are

TABLE I. Decay branching ratios (in %) for top squarks and bottom squarks in the two considered scenarios. Corresponding values of the underlying MSSM parameters are given in the text.

	Scenario with $\tan\beta=6$				Scenario with $\tan\beta=30$			
Channel	$\tilde{t}_1$	$\tilde{t}_2$	$\tilde{b}_1$	$\tilde{b}_2$	$\tilde{t}_1$	$\tilde{t}_2$	$\tilde{b}_1$	$\tilde{b}_2$
$q\tilde{\chi}_1^0$	66.4	1.6	100	0.6	0	0.6	63.5	0.6
$q\tilde{\chi}_2^0$	0	7.5	0	8.7	0	8.5	36.1	10.3
$q\tilde{\chi}_3^0$	0	13.1	0	0.3	0	11.1	0	4.6
$q\tilde{\chi}_4^0$	0	6.6	0	2.4	0	8.7	0	4.6
$q'\tilde{\chi}_1^\pm$	33.1	19.2	0	9.7	100	22.5	0	14.1
$q'\tilde{\chi}_2^\pm$	0	1.6	0	21.0	0	6.8	0	24.2
$W^\pm\tilde{q}_1'$	0.5	0.3	0	56.8	0	3.1	0.4	27.1
$H^\pm\tilde{q}_1'$	0	0	0	0	0	7.7	0	6.4
$Z\tilde{q}_1$	–	26.9	–	0.2	–	13.1	–	1.5
$H_1\tilde{q}_1$	–	23.4	–	0.2	–	12.7	–	1.4
$H_2\tilde{q}_1$	–	0	–	0	–	2.8	–	2.7
$H_3\tilde{q}_1$	–	0	–	0	–	2.4	–	2.7

$m_{\tilde{\chi}_1^\pm}=(278.5\pm0.2)$ GeV, $m_{\tilde{\chi}_2^\pm}=(384.5\pm0.3)$ GeV, $m_{\tilde{\chi}_1^0}=(148.7\pm0.3)$ GeV, $m_{\tilde{\chi}_2^0}=(277.8\pm0.5)$ GeV, $m_{\tilde{\chi}_3^0}=(359.1\pm0.3)$ GeV, $m_{\tilde{\chi}_4^0}=(382.0\pm0.7)$ GeV, $m_{H_1}=(115.47\pm0.05)$ GeV, $m_{H_2}=(896.5\pm9.0)$ GeV, $m_{H_3}=(897.1\pm9.0)$ GeV, $m_{\tilde{t}_1}=(350.0\pm3.5)$ GeV, $m_{\tilde{t}_2}=(700.0\pm21.0)$ GeV, $m_{\tilde{b}_1}=(170.0\pm1.7)$ GeV, and $m_{\tilde{b}_2}=(626.0\pm19.0)$ GeV. Moreover, we find $B(b\to s\gamma)=3.6\times10^{-4}$. The corresponding top squark and bottom squark branching ratios are given in Table I. The large $\tan\beta$ scenario is specified by $M_{\tilde{D}}=360.0$ GeV, $M_{\tilde{U}}=198.2$ GeV, $M_{\tilde{Q}}=691.9$ GeV, $|A_t|=600$ GeV, $\varphi_{A_t}=\pi/4$, $|A_b|=1000$ GeV, $\varphi_{A_b}=3\pi/2$, $\varphi_{U(1)}=0$, $M_2=200$ GeV, $\mu=-350$ GeV, $\tan\beta=30$, $m_{\tilde{g}}=1000$ GeV, and $m_{H^\pm}=350$ GeV. The resulting masses and their assumed errors are $m_{\tilde{\chi}_1^\pm}=(188.2\pm0.5)$ GeV, $m_{\tilde{\chi}_2^\pm}=(374.2\pm0.9)$ GeV, $m_{\tilde{\chi}_1^0}=(98.2\pm0.6)$ GeV, $m_{\tilde{\chi}_2^0}=(188.2\pm0.9)$ GeV, $m_{\tilde{\chi}_3^0}=(358.5\pm0.9)$ GeV, $m_{\tilde{\chi}_4^0}=(371.6\pm2.0)$ GeV, $m_{H_1}=(113.63\pm0.05)$ GeV, $m_{H_2}=(340.7\pm1.5)$ GeV, $m_{H_3}=(341.1\pm1.5)$ GeV, $m_{\tilde{t}_1}=(210.0\pm2.1)$ GeV, $m_{\tilde{t}_2}=(729.0\pm22.0)$ GeV, $m_{\tilde{b}_1}=(350.0\pm3.5)$ GeV, and $m_{\tilde{b}_2}=(700.0\pm21.0)$ GeV. Moreover, we have $B(b\to s\gamma)=4.4\times10^{-4}$. The corresponding top squark and bottom squark branching ratios are given in Table I. We have chosen a relatively small $\tilde{b}_1$ mass in the small $\tan\beta$ scenario and a relatively small $\tilde{t}_1$ mass in the large $\tan\beta$ scenario. As a result of this in the two scenarios considered the observables in the $\tilde{t}_i$ and $\tilde{b}_i$ sectors are sufficient to determine all $\tilde{t}_i$ and $\tilde{b}_i$ parameters.

We have taken the relative errors of chargino and neutralino masses from Refs. [54,55], which we rescale according to our scenario; in case of $\tan\beta=30$ we have taken into account an additional factor of 3 for the errors (relatively to $\tan\beta=6$) due to the reduced efficiency in case of multi-τ final states from decays of charginos and neutralinos as indicated by the studies in Ref. [7].

A detailed Monte Carlo study of the $\tilde{t}_1$ production $e^+e^-\to\tilde{t}_1\bar{\tilde{t}}_1$ and the $\tilde{t}_1$ decays $\tilde{t}_1\to c\tilde{\chi}_1^0$ and $\tilde{t}_1\to b\tilde{\chi}_1^+$ at TESLA ($\sqrt{s}=500$ GeV and $\mathcal{L}=500$ fb^{-1}) has been performed in Ref. [10] for real MSSM parameters. These results cannot directly be used for our error analysis, because we consider additional $\tilde{t}_1$ and $\tilde{t}_2$ decays. To the best of our knowledge no Monte Carlo studies exist that include all of the $\tilde{t}_1$ and $\tilde{t}_2$ decays considered in our analysis. Therefore, we have taken only statistical errors for the production cross sections and branching ratios by calculating the corresponding number of events for the decay $\tilde{t}_1\to X$ as

$$N=2\mathcal{L}[\sigma(\tilde{t}_1\bar{\tilde{t}}_1)+\sigma(\tilde{t}_1\bar{\tilde{t}}_2)]B(\tilde{t}_1\to X) \tag{45}$$

and analogously for $\tilde{t}_2$, $\tilde{b}_1$, and $\tilde{b}_2$ decays. For definiteness we take an integrated luminosity $\mathcal{L}=1$ ab^{-1} at a center of mass system (c.m.s.) energy $\sqrt{s}=2$ TeV (i.e., at CLIC). We do not take systematic experimental errors for the cross sections and branching ratios into account since we are not aware of any study considering the systematic errors. Instead we have doubled the statistical errors obtained above. The evaluation of the systematic experimental errors would require further Monte Carlo studies for a specific linear collider which, however, are beyond the scope of our paper.

For the determination of the squark parameters we have used the information obtained from the measurement of the squark masses at threshold and the squark production cross sections at $\sqrt{s}=2$ TeV for two different (e^-,e^+) beam polarizations $(P_-,P_+)=(0.8,-0.4)$ and $(P_-,P_+)=(-0.8,0.4)$. Here we have assumed that a total effective luminosity of 1 ab^{-1} is available for each choice of polarization. The cross section measurements are important for the determination of $|\cos\theta_t|^2$ and $|\cos\theta_b|^2$ as can be seen from Eq. (25) and the formulas for the cross sections in Ref. [9]. In the numerical evaluation of the squark production

TABLE II. Extracted parameters from the ''experimental data'' of the masses, production cross sections, and decay branching ratios of $\tilde{t}_i$ and $\tilde{b}_i$. The original parameters for each scenario are given in the text.

Scenario	$\tan\beta=6$ scenario	$\tan\beta=30$ scenario
$M^2_{\tilde{D}}$	$(2.88\pm0.06)\times10^4$	$(1.30\pm0.02)\times10^5$
$M^2_{\tilde{U}}$	$(1.67\pm0.04)\times10^5$	$(3.93\pm0.12)\times10^4$
$M^2_{\tilde{Q}}$	$(3.88\pm0.04)\times10^5$	$(4.79\pm0.04)\times10^5$
$\mathrm{Re}(A_t)$	565.0 ± 13.0	424.0 ± 14.0
$\mathrm{Im}(A_t)$	$\pm566.0\pm14.0$	$\pm425.0\pm15.0$
$\mathrm{Re}(A_b)$	620.0 ± 190.0	6.5 ± 420.0
$\mathrm{Im}(A_b)$	$\pm230.0\pm580.0$	$\pm999.0\pm52.0$
$\mathrm{Re}(M_1)$	149.3 ± 0.3	99.6 ± 0.6
$\mathrm{Im}(M_1)$	1.0 ± 1.5	-0.5 ± 2.8
M_2	300.0 ± 0.4	200.0 ± 0.5
$\mathrm{Re}(\mu)$	-350.0 ± 0.3	-350.0 ± 0.6
$\mathrm{Im}(\mu)$	-0.02 ± 0.9	1.5 ± 5.0
$\tan\beta$	6.0 ± 0.2	30.0 ± 0.8
$m_{\tilde{g}}$	1000.0 ± 30	1000.0 ± 30
$m_{H^\pm}$	900.0 ± 5.0	350.0 ± 0.8

cross sections we have included initial state radiation according to Ref. [60]. In addition we have used the information from all branching ratios in Table I with the corresponding statistical errors. These branching ratios together with the masses and cross sections form an overconstraining system of observables for the underlying parameters $M^2_{\tilde{D}}$, $M^2_{\tilde{U}}$, $M^2_{\tilde{Q}}$, $\mathrm{Re}(A_t)$, $\mathrm{Im}(A_t)$, $\mathrm{Re}(A_b)$, $\mathrm{Im}(A_b)$, $\mathrm{Re}(M_1)$, $\mathrm{Im}(M_1)$, M_2, $\mathrm{Re}(\mu)$, $\mathrm{Im}(\mu)$, $\tan\beta$, $m_{\tilde{g}}$, and $m_{H^\pm}$. The latter two enter the formulas for the neutral Higgs masses and mixing. We determine these parameters and their errors from the ''experimental data'' on these observables by a least-square fit. The results obtained are shown in Table II. Note that the sign ambiguity for the imaginary parts of the parameters is due to the fact that we consider *CP*-even observables. This ambiguity can in principle be resolved by considering appropriate *CP*-odd observables (as proposed in Refs. [20–22]) in the analysis. As one can see, all parameters except A_b can be determined rather precisely. $\tan\beta$ can be determined with an error of about 3% in both scenarios. The relative error of the squark mass parameters squared is in the range of 1% to 2%. A_t can be measured within an error of 2–3 % independently of $\tan\beta$. The reasons for this are (i) the mixing angle in the top squark sector, which can be measured rather precisely using polarized $e^\pm$ beams, depends strongly on A_t and (ii) A_t influences strongly the corrections to the mass of the lightest Higgs boson. The situation for A_b is considerably worse: in case of small $\tan\beta$ one gets only an order of magnitude estimate. The reason is that both the bottom squark mixing angle and the bottom squark couplings depend only weakly on A_b for small $\tan\beta$. In case of large $\tan\beta$ the situation improves somewhat in particular for the imaginary part of A_b. The main sources of information on A_b are the branching ratios of the decays of the heavier bottom squark into a Higgs boson plus the lighter bottom squark because the corresponding couplings depend significantly on A_b [see Eqs. (35)–(37)]. From this we conclude that the situation for A_b improves in scenarios where these branching ratios are large. An additional source of information could be the polarization information of the fermions in bottom squark decays as proposed in Ref. [12]. We have found that the analogous fit procedure for real MSSM parameters gives a larger value for χ^2: $\Delta\chi^2=286.6$ for the scenario with $\tan\beta=6$ and $\Delta\chi^2=22.5$ for the scenario with $\tan\beta=30$. In Table II most of the central values of the fitted parameters are the same as their input values because we have taken the observables calculated from the input parameters as ''experimental data.'' We have checked that a shift within 1σ of the ''experimental data'' leads to almost no change of the errors of the parameters.

The results presented in Table II depend clearly on the assumed experimental errors which have been summarized in the beginning of this section. It is clear that further detailed Monte Carlo studies including experimental cuts and detector simulation are necessary to determine more accurately the expected experimental errors of the observables for our scenarios, in particular the errors of the top squark and bottom squark decay branching ratios. Such a study is, however, beyond the scope of this paper. Furthermore, an additional source of uncertainty is the theoretical error due to higher order corrections etc. [43,44]. We have not taken into account these effects because most formulas given in the literature are only for real parameters. Instead we have studied how our results for the errors of the fundamental parameters are changed when the experimental errors of the various observables are changed: we have redone the procedure doubling the errors of the masses and/or branching ratios and/or cross sections. We find that the errors of all parameters are approximately doubled if all experimental errors are

doubled. Moreover, in this way we can see to which observables an individual parameter is most sensitive. We find that precision on the top squark parameters $A_t, M^2_{\tilde{Q}}$, and $M^2_{\tilde{U}}$ is sensitive to the accuracy of the top squark mass measurement at the threshold as well as to the precision of the measurement of the total top squark pair production cross sections in the continuum using polarized $e^{\pm}$ beams. The error of A_t is also very sensitive to the error of the lightest Higgs boson mass due to the large top squark loop corrections. The precision on the parameters $M^2_{\tilde{D}}$ and $M^2_{\tilde{Q}}$ is sensitive to the accuracy of the bottom squark mass measurement. The accuracy of A_b is most sensitive to the precision of the measurements of the branching ratios for the bottom squark (and top squark) decays into Higgs bosons. The precision of μ is more sensitive to the errors of chargino and neutralino masses than to the errors of the top squark and bottom squark observables. In the case of large $\tan\beta$, the precision of $\tan\beta$ depends to some extent on the precision of the bottom squark pair production cross sections and to a lesser extent also on that of the bottom squark decay branching ratios.

For the determination of the $\tilde{t}_i$ and $\tilde{b}_i$ parameters the measurements of the branching ratios of the squark decays into Higgs bosons together with those of the squark mixing angles from the production cross sections are important. Therefore, we need to obtain information about $\tilde{t}_1$, $\tilde{t}_2$, $\tilde{b}_1$, and $\tilde{b}_2$ production and decays separately. This can be achieved at a linear collider by suitable choices of the c.m.s. energy. We note that, in the case $m_{\tilde{t}_2}, m_{\tilde{b}_2} \gtrsim 500$ GeV, the measurements of the cross sections, masses, and branching ratios of $\tilde{t}_2$ and $\tilde{b}_2$ at an e^+e^- linear collider with $\sqrt{s} = 2$ TeV are necessary for the determination of A_t and A_b; otherwise this might not be possible. However, additional information from the LHC on the $\tilde{t}_i$ and $\tilde{b}_i$ masses and some of the decay channels would certainly improve the situation. In the error estimate presented here we have assumed that many decay channels of the $\tilde{t}_i$ and $\tilde{b}_i$ are open. If this is not the case, then the missing information could be obtained by studying the decay properties of the heavier charginos, neutralinos, and Higgs bosons into $\tilde{t}_i$ and $\tilde{b}_i$.

V. SUMMARY

In this paper we have studied the decays of top squarks $\tilde{t}_i$ and bottom squarks $\tilde{b}_i$ in the MSSM with complex parameters A_t, A_b, μ, and M_1. We have taken into account the explicit *CP* violation in the Higgs sector induced by $\tilde{t}_i$ and $\tilde{b}_i$ loops in the case $A_{t,b}$ and μ are complex. We have presented numerical results for the fermionic and bosonic decay branching ratios of $\tilde{t}_i$ and $\tilde{b}_i (i = 1,2)$. We have analyzed their MSSM parameter dependence, in particular the dependence on the *CP* phases φ_{A_t}, φ_{A_b}, φ_μ, and $\varphi_{\mathrm{U}(1)}$. We have found that the experimental data of the branching ratio of the decay $b \to s\gamma$ can lead to considerable restrictions on the MSSM parameter space. In the case of $\tilde{t}_i$ decays the strong dependence on φ_{A_t} and φ_μ is due to the phase dependence of the mixing angle $\theta_{\tilde{t}}$, of the mixing phase factor $e^{i\varphi_{\tilde{t}}}$ and of the Higgs couplings G_{12} $(= C^H_{\tilde{b}_R \tilde{t}_L})$, G_{21} $(= C^H_{\tilde{b}_L \tilde{t}_R})$, and $C(\tilde{t}^\dagger_L H_i \tilde{t}_R)$. In the case of $\tilde{b}_i$ decays there can be a strong φ_{A_b} dependence if $\tan\beta$ is large and the decays into Higgs bosons are allowed. If the parameters A_t, A_b, μ, and M_1 are complex and there is mixing between the *CP*-even and *CP*-odd Higgs bosons, the decay pattern of $\tilde{t}_i$ and $\tilde{b}_i$ is even more complicated than that in the case of real parameters. This could have important implications for $\tilde{t}_i$ and $\tilde{b}_i$ searches at future colliders and the determination of the underlying MSSM parameters.

We have also estimated what accuracy can be expected in the determination of the underlying MSSM parameters by a global fit of the observables (masses, branching ratios, and production cross sections) measured at typical linear colliders with polarized beams. We have considered two scenarios with $\tan\beta = 6$ and $\tan\beta = 30$. Under favorable conditions the fundamental MSSM parameters except $A_{t,b}$ can be determined with errors of 1% to 2%, assuming an integrated luminosity of 1 ab^{-1}. The parameter A_t can be determined within an error of 2–3% whereas the error of A_b is likely to be of the order of 50%.

ACKNOWLEDGMENTS

We thank M. Battaglia, A. De Roeck, H. Eberl, M. Krämer, W. Majerotto, G. Moortgat-Pick, and G. Weiglein for useful discussions. K. H. appreciates valuable discussions with E. Berger, H. Haber, G. Kane, and P. Nath. This work is supported by the ''Fonds zur Förderung der wissenschaftlichen Forschung'' of Austria, FWF Projects No. P13139-PHY and No. P16592-N02 and by the European Community's Human Potential Program under contract HPRN-CT-2000-00149. W.P. has been supported by the Erwin Schrödinger Grant No. J2272 of the ''Fonds zur Förderung der wissenschaftlichen Forschung'' of Austria and partly by the Swiss ''Nationalfonds.''

APPENDIX

Masses and mixing in the neutral higgs sector

In the complex MSSM the explicit *CP* violation in the Higgs sector is mainly induced by $\tilde{t}$ and $\tilde{b}$ loops resulting in a 3×3 neutral Higgs mass matrix with a mixing of the *CP*-even Higgs bosons ϕ_1 and ϕ_2 and the *CP*-odd Higgs boson *a*. At one-loop level the amount of mixing of *CP*-even and *CP*-odd Higgs states is approximately proportional to $\sin(\varphi_{A_{t,b}} + \varphi_\mu)$. The three neutral mass eigenstates are denoted as $H_i (i = 1,2,3)$ with masses $m_{H_1} < m_{H_2} < m_{H_3}$ (following the notation of Ref. [28]). The real orthogonal mixing matrix in the neutral Higgs sector is denoted by a 3×3 matrix *O*:

$$\begin{pmatrix} H_1 \\ H_2 \\ H_3 \end{pmatrix} = O^T \begin{pmatrix} \phi_1 \\ \phi_2 \\ a \end{pmatrix}, \tag{A1}$$

where ϕ_1, ϕ_2, and a are related to the neutral entries of the two Higgs doublet fields by $H_1^0=(1/\sqrt{2})(v_1+\phi_1-ia_1)$, $H_2^0=(1/\sqrt{2})(v_2+\phi_2+ia_2)$, and $a=-\sin\beta a_1+\cos\beta a_2$. We take the parameter $\xi=0$ as in Ref. [28]. We have included the full one-loop corrections to the Higgs mass eigenvalues m_{H_i} and the mixing matrix O_{ij} as implemented in the program FEYNHIGGS2.0.2 [30]. We use these results for m_{H_i} and O_{ij} in our tree-level formula for the $\tilde{t}_2$, $\tilde{b}_2$ decay widths [Eq. (42)] and in the constraint (ii).

Chargino masses and mixing

At tree level the chargino mass matrix in the weak basis is given by [1,61]

$$\mathcal{M}_C=\begin{pmatrix} M_2 & \sqrt{2}m_W s_\beta \\ \sqrt{2}m_W c_\beta & |\mu|e^{i\varphi_\mu} \end{pmatrix}. \tag{A2}$$

c_β and s_β are $\cos\beta$ and $\sin\beta$, respectively. This complex 2×2 matrix is diagonalized by the unitary 2×2 matrices U and V:

$$U^*\mathcal{M}_C V^\dagger=\mathrm{diag}(m_{\tilde{\chi}_1^\pm},m_{\tilde{\chi}_2^\pm}),\quad 0\leqslant m_{\tilde{\chi}_1^\pm}\leqslant m_{\tilde{\chi}_2^\pm}. \tag{A3}$$

We have neglected one-loop corrections to the chargino mass matrix $\mathcal{M}_C$, as have been given in Refs. [44,62] for real parameters.

Neutralino masses and mixing

At tree level the neutralino mass matrix in the weak basis $(\tilde{B},\tilde{W}^3,\tilde{H}_1^0,\tilde{H}_2^0)$ is given as [1,61]:

$$\mathcal{M}_N=\begin{pmatrix} |M_1|e^{i\varphi_{\mathrm{U}(1)}} & 0 & -m_Z s_W c_\beta & m_Z s_W s_\beta \\ 0 & M_2 & m_Z c_W c_\beta & -m_Z c_W s_\beta \\ -m_Z s_W c_\beta & m_Z c_W c_\beta & 0 & -|\mu|e^{i\varphi_\mu} \\ m_Z s_W s_\beta & -m_Z c_W s_\beta & -|\mu|e^{i\varphi_\mu} & 0 \end{pmatrix}, \tag{A4}$$

where $\varphi_{\mathrm{U}(1)}$ is the phase of M_1, and c_W and s_W are $\cos\theta_W$ and $\sin\theta_W$, respectively. This symmetric complex mass matrix is diagonalized by the unitary 4×4 matrix N:

$$N^*\mathcal{M}_N N^\dagger=\mathrm{diag}(m_{\tilde{\chi}_1^0},\ldots,m_{\tilde{\chi}_4^0}),\quad 0\leqslant m_{\tilde{\chi}_1^0}\leqslant\ldots\leqslant m_{\tilde{\chi}_4^0}. \tag{A5}$$

We have not included one-loop corrections to the neutralino mass matrix $\mathcal{M}_N$, like those given in Refs. [44,62] for real parameters.

[1] For reviews, see: H.P. Nilles, Phys. Rep. **110**, 1 (1984); H.E. Haber and G.L. Kane, *ibid.* **117**, 75 (1985); R. Barbieri, Riv. Nuovo Cimento **11**, 1 (1988).

[2] M. Dugan, B. Grinstein, and L.J. Hall, Nucl. Phys. **B255**, 413 (1985).

[3] A. Masiero and O. Vives, New J. Phys. **4**, 4 (2002).

[4] F. Csikor, Z. Fodor, and J. Heitger, Phys. Rev. Lett. **82**, 21 (1999).

[5] H. Baer, M. Drees, R. Godbole, J.F. Gunion, and X. Tata, Phys. Rev. D **44**, 725 (1991); H. Baer, J. Sender, and X. Tata, *ibid.* **50**, 4517 (1994).

[6] M.M. Nojiri, Phys. Rev. D **51**, 6281 (1995).

[7] M.M. Nojiri, K. Fujii, and T. Tsukamoto, Phys. Rev. D **54**, 6756 (1996).

[8] A. Bartl, H. Eberl, S. Kraml, W. Majerotto, W. Porod, and A. Sopczak, Z. Phys. C **76**, 549 (1997).

[9] A. Bartl, H. Eberl, S. Kraml, W. Majerotto, and W. Porod, Eur. Phys. J. C **2**, 6 (2000).

[10] R. Keranen, A. Sopczak, H. Nowak, and M. Berggren, Eur. Phys. J. C **7**, 1 (2000); A. Finch, H. Nowak, and A. Sopczak, in *Physics and Experiments with Future Electron-Positron Linear Colliders*, edited by J.S. Kang and S.K. Oh (Korean Physical Society, Korea, 2003), p. 820. hep-ph/0211140.

[11] E. Boos, G. Moortgat-Pick, H.U. Martyn, M. Sachwitz, and A. Vologdin, in *Supersymmetry and Unification of Fundamental Interactions*, Hamburg, 2002, edited by P. Nath, P.M. Zerwas, and C. Grosche (DESY, Hamburg, 2002), Vol. 2, pp. 938–949. hep-ph/0211040.

[12] E. Boos, H.U. Martyn, G. Moortgat-Pick, M. Sachwitz, A. Sherstnev, and P.M. Zerwas, Eur. Phys. J. C **30**, 395 (2003).

[13] A. Bartl, W. Majerotto, and W. Porod, Z. Phys. C **64**, 499 (1994); **68**, 518(E) (1995).

[14] H. Baer, C.H. Chen, M. Drees, F. Paige, and X. Tata, Phys. Rev. Lett. **79**, 986 (1997); Phys. Rev. D **59**, 055014 (1999).

[15] J. Hisano, K. Kawagoe, R. Kitano, and M.M. Nojiri, Phys. Rev. D **66**, 115004 (2002); J. Hisano, K. Kawagoe, and M.M. Nojiri, *ibid.* **68**, 035007 (2003); U. Dydak, Diploma thesis, Univ. Vienna (1996); *'96 QCD and High Energy Hadronic Interactions: Proceedings*, edited by J. Tran Tranh Van (Editions Frontieres, Gif-sur-Yvette, France, 1996), pp. 599–604.

[16] F.E. Paige, in *20 years of SUGRA, Boston 2003*, edited by P. Nath (Rinton Press, Princeton, NJ, 2004), pp. 76–92, hep-ph/0307342.

[17] A. Bartl, H. Eberl, K. Hidaka, S. Kraml, T. Kon, W. Majerotto, W. Porod, and Y. Yamada, Phys. Lett. B **435**, 118 (1998); **460**, 157 (1999).

[18] K. Hidaka and A. Bartl, Phys. Lett. B **501**, 78 (2001).

[19] C. Weber, H. Eberl, and W. Majerotto, Phys. Lett. B **572**, 56 (2003).

[20] M. Aoki and N. Oshimo, Mod. Phys. Lett. A **13**, 3225 (1998); W.M. Yang and D.S. Du, Phys. Rev. D **65**, 115005 (2002).

[21] A. Bartl, T. Kernreiter, and W. Porod, Phys. Lett. B **538**, 59 (2002).

[22] A. Bartl, H. Fraas, T. Kernreiter, and O. Kittel, Eur. Phys. J. C **33**, 433 (2004).

[23] D.A. Demir, Phys. Rev. D **60**, 055006 (1999).
[24] S.Y. Choi and J.S. Lee, Phys. Rev. D **61**, 015003 (2000); S.Y. Choi, K. Hagiwara, and J.S. Lee, *ibid.* **64**, 032004 (2001).
[25] M. Carena, J.R. Ellis, A. Pilaftsis, and C.E. Wagner, Phys. Lett. B **495**, 155 (2000).
[26] A. Bartl, K. Hidaka, T. Kernreiter, and W. Porod, Phys. Lett. B **538**, 137 (2002); Phys. Rev. D **66**, 115009 (2002).
[27] T. Ibrahim and P. Nath, Phys. Rev. D **67**, 095003 (2003); **68**, 019901(E) (2003).
[28] M. Carena, J.R. Ellis, A. Pilaftsis, and C.E. Wagner, Nucl. Phys. **B586**, 92 (2000).
[29] A. Pilaftsis, Phys. Lett. B **435**, 88 (1998); A. Pilaftsis and C.E. Wagner, Nucl. Phys. **B553**, 3 (1999); S.Y. Choi, M. Drees, and J.S. Lee, Phys. Lett. B **481**, 57 (2000); G.L. Kane and L.T. Wang, *ibid.* **488**, 383 (2000); M. Carena, J.R. Ellis, A. Pilaftsis, and C.E. Wagner, Nucl. Phys. **B625**, 345 (2002).
[30] S. Heinemeyer, Eur. Phys. J. C **22**, 521 (2001); M. Frank, S. Heinemeyer, W. Hollik, and G. Weiglein, in *Supersymmetry and Unification of Fundamental Interactions*, *Hamburg 2002*, edited by P. Nath, P.M. Zerwas, and C. Grosche (DESY, Hamburg, 2002), Vol. 2, pp. 637–647, hep-ph/0212037; see also http://www.feynhiggs.de/
[31] M. Carena, J.R. Ellis, S. Mrenna, A. Pilaftsis, and C.E. Wagner, Nucl. Phys. **B659**, 145 (2003).
[32] J.R. Ellis, S. Ferrara, and D.V. Nanopoulos, Phys. Lett. **114B**, 231 (1982); W. Buchmüller and D. Wyler, *ibid.* **121B**, 321 (1983); J. Polchinski and M.B. Wise, *ibid.* **125B**, 393 (1983); J.M. Gerard, W. Grimus, A. Masiero, D.V. Nanopoulos, and A. Raychaudhuri, Nucl. Phys. **B253**, 93 (1985); P. Nath, Phys. Rev. Lett. **66**, 2565 (1991); Y. Kizukuri and N. Oshimo, Phys. Rev. D **45**, 1806 (1992); **46**, 3025 (1992); T. Falk and K.A. Olive, Phys. Lett. B **375**, 196 (1996).
[33] V.D. Barger, T. Falk, T. Han, J. Jiang, T. Li, and T. Plehn, Phys. Rev. D **64**, 056007 (2001).
[34] T. Ibrahim and P. Nath, Phys. Lett. B **418**, 98 (1998); Phys. Rev. D **57**, 478 (1998); **58**, 019901(E) (1998); **60**, 079903(E) (1999); **60**, 119901 (1999); **58**, 111301 (1998); **60**, 099902(E) (1999); **61**, 093004 (2000); M. Brhlik, G.J. Good, and G.L. Kane, *ibid.* **59**, 115004 (1999); M. Brhlik, L.L. Everett, G.L. Kane, and J. Lykken, Phys. Rev. Lett. **83**, 2124 (1999); Phys. Rev. D **62**, 035005 (2000); A. Bartl, T. Gajdosik, W. Porod, P. Stockinger, and H. Stremnitzer, *ibid.* **60**, 073003 (1999); A. Bartl, T. Gajdosik, E. Lunghi, A. Masiero, W. Porod, H. Stremnitzer, and O. Vives, *ibid.* **64**, 076009 (2001); S. Abel, S. Khalil, and O. Lebedev, Nucl. Phys. **B606**, 151 (2001).
[35] A.G. Cohen, D.B. Kaplan, and A.E. Nelson, Phys. Lett. B **388**, 588 (1996); A.G. Akeroyd, Y.Y. Keum, and S. Recksiegel, *ibid.* **507**, 252 (2001) and references therein.
[36] A. Bartl, W. Majerotto, W. Porod, and D. Wyler, Phys. Rev. D **68**, 053005 (2003).
[37] D. Chang, W.Y. Keung, and A. Pilaftsis, Phys. Rev. Lett. **82**, 900 (1999); **83**, 3972(E) (1999); A. Pilaftsis, Phys. Lett. B **471**, 174 (1999); D. Chang, W.F. Chang, and W.Y. Keung, *ibid.* **478**, 239 (2000); A. Pilaftsis, Nucl. Phys. **B644**, 263 (2002).
[38] A. Bartl, S. Hesselbach, K. Hidaka, T. Kernreiter, and W. Porod, ''Contribution to the extended joint ECFA/DESY Study on Physics and Detectors for a Linear Electron-Positron Collider,'' Report No. LC-TH-2003-041, hep-ph/0306281; Phys. Lett. B **573**, 153 (2003).
[39] Belle Collaboration, K. Abe *et al.*, Phys. Lett. B **511**, 151 (2001); Cleo Collaboration, S. Chen *et al.*, Phys. Rev. Lett. **87**, 251807 (2001); BABAR Collaboration, B. Aubert *et al.*, *ibid.* **88**, 101805 (2002); Cleo Collaboration, E.H. Thorndike hep-ex/0206067.
[40] A. Arhrib, M. Capdequi-Peyranere, and A. Djouadi, Phys. Rev. D **52**, 1404 (1995); H. Eberl, A. Bartl, and W. Majerotto, Nucl. Phys. **B472**, 481 (1996); H. Eberl, S. Kraml, and W. Majerotto, J. High Energy Phys. **5**, 016 (1999); A. Arhrib and W. Hollik, *ibid.* **4**, 073 (2004).
[41] H. Eberl, K. Hidaka, S. Kraml, W. Majerotto, and Y. Yamada, Phys. Rev. D **62**, 055006 (2000).
[42] M. Carena, S. Mrenna, and C.E. Wagner, Phys. Rev. D **60**, 075010 (1999); M. Carena, D. Garcia, U. Nierste, and C.E. Wagner, Nucl. Phys. **B577**, 88 (2000); H.E. Logan, Nucl. Phys. B (Proc. Suppl.) **101**, 279 (2001); H. Baer, J. Ferrandis, K. Melnikov, and X. Tata, Phys. Rev. D **66**, 074007 (2002); C. Pallis, Nucl. Phys. **B678**, 398 (2004); S. Profumo, Phys. Rev. D **68**, 015006 (2003).
[43] S. Kraml, H. Eberl, A. Bartl, W. Majerotto, and W. Porod, Phys. Lett. B **386**, 175 (1996); A. Djouadi, W. Hollik, and C. Junger, Phys. Rev. D **55**, 6975 (1997); A. Bartl, H. Eberl, K. Hidaka, S. Kraml, W. Majerotto, W. Porod, and Y. Yamada, Phys. Lett. B **419**, 243 (1998); A. Bartl, H. Eberl, K. Hidaka, S. Kraml, W. Majerotto, W. Porod, and Y. Yamada, Phys. Rev. D **59**, 115007 (1999); J. Guasch, J. Sola, and W. Hollik, Phys. Lett. B **437**, 88 (1998); J. Guasch, W. Hollik, and J. Sola, *ibid.* **510**, 211 (2001).
[44] J. Guasch, W. Hollik, and J. Sola, J. High Energy Phys. **10**, 040 (2002).
[45] ALEPH Collaboration, A. Heister *et al.*, Phys. Lett. B **526**, 191 (2002).
[46] M. Drees and K. Hagiwara, Phys. Rev. D **42**, 1709 (1990); G. Altarelli, R. Barbieri, and F. Caravaglios, Int. J. Mod. Phys. A **13**, 1031 (1998); S.K. Kang and J.D. Kim, Phys. Rev. D **62**, 071901 (2000).
[47] ALEPH Collaboration, A. Heister *et al.*, Phys. Lett. B **537**, 5 (2002); G. Sguazzoni, in *ICHEP 2002*, *Proceedings of the 31st International Conference on High Energy Physics*, *Amsterdam*, *The Netherlands*, *2002*, edited by S. Bentvelson, P. de Jong, J. Koch, and E. Laenen (North-Holland, The Netherlands, 2003), p. 709.
[48] LEP Higgs Working Group Collaboration, Int. J. Mod. Phys. A **17**, 22 (2002); DELPHI Collaboration, J. Abdallah *et al.*, Eur. Phys. J. C **23**, 409 (2002); L3 Collaboration, P. Achard *et al.*, Phys. Lett. B **545**, 30 (2002); P. Lutz, in *ICHEP 2002*, *Proceedings of the 31st International Conference on High Energy Physics*, *Amsterdam*, *The Netherlands*, *2002*, edited by S. Bentvelson, P. de Jong, J. Koch, and E. Laenen (North-Holland, The Netherlands, 2003), p. 735; LEP Collaboration, P. Bechtle, hep-ex/0401007.
[49] S. Bertolini, F. Borzumati, A. Masiero, and G. Ridolfi, Nucl. Phys. **B353**, 591 (1991).
[50] A.L. Kagan and M. Neubert, Eur. Phys. J. C **7**, 5 (1999).
[51] J.P. Derendinger and C.A. Savoy, Nucl. Phys. **B237**, 307 (1984); J.A. Casas and S. Dimopoulos, Phys. Lett. B **387**, 107 (1996).
[52] S. Bae, Phys. Lett. B **489**, 171 (2000).
[53] A. De Roeck (private communication).

[54] ECFA/DESY LC Physics Working Group Collaboration, J.A. Aguilar-Saavedra *et al.*, ''Tesla: The Superconducting Electron Positron Linear Collider with an Integrated X-ray Laser Laboratory, Technical Design Report, 3, Physics at an $E_+ E_-$ Linear Collider,'' hep-ph/0106315; E. Accomando *et al.*, Phys. Rep. **229**, 1 (1998); H. Murayama and M.E. Peskin, Annu. Rev. Nucl. Part. Sci. **46**, 533 (1996); J.L. Feng and M.M. Nojiri, in *Linear Collider Physics in the New Millenium*, edited by David Miller, Feisuke Fujii, and Amarjit Soni (World Scientific, Singapore, 2002), hep-ph/0210390.

[55] H.U. Martyn and G.A. Blair, in Proceedings of the *4th International Workshop on Linear Colliders (LCWS 99), Sitges, Barcelona, Spain, 1999*, hep-ph/9910416.

[56] S. Heinemeyer, S. Kraml, W. Porod, and G. Weiglein, J. High Energy Phys. **09**, 075 (2003).

[57] M. Battaglia (private communication).

[58] G. Polesello (private communication).

[59] F. James and M. Roos, Comput. Phys. Commun. **10**, 343 (1975).

[60] E.A. Kuraev and V.S. Fadin, Yad Fiz. **41**, 733 (1985) [Sov. J. Nucl. Phys. **41**, 466 (1985)]; M. E. Peskin, SLAC Report No. SLAC-PUB-5210, in *Physics at the 100 GeV Mass Scale*, 17th SLAC Summer Institute, Stanford, CA, 1989, p. 71.

[61] J.F. Gunion and H.E. Haber, Nucl. Phys. **B272**, 1 (1986); **B402**, 567(E) (1993); **B278**, 449 (1986).

[62] H. Eberl, M. Kincel, W. Majerotto, and Y. Yamada, Phys. Rev. D **64**, 115013 (2001); T. Fritzsche and W. Hollik, Eur. Phys. J. C **24**, 619 (2002); W. Öller, H. Eberl, W. Majerotto, and C. Weber, *ibid.* **29**, 563 (2003).